CHAPTER IV
RESULT AND DISCUSSION

4.1 BET surface area

4.1.1 The effect of urea concentrations on BET surface area of $Ce_{0.75}Zr_{0.25}O_2$

$Ce_{0.75}Zr_{0.25}O_2$ catalysts were prepared by urea hydrolysis. The urea concentration were varied from 0.4M, 1M and 2M. BET surface areas of $Ce_{0.75}Zr_{0.25}O_2$ with different urea conentrations measured by multiple point BET method. Table 4.1 shows BET surface area of $Ce_{0.75}Zr_{0.25}O_2$ with different urea concentrations for both calcined temperatures at 500°C and 900°C.

BET surface areas of $Ce_{0.75}Zr_{0.25}O_2$ prepared by different urea concentrations are not significantly different. The shapes of each sample are also similar. They are spherical shapes composed with long thin needle shape. Therefore, the urea concentration of 0.4M was selected for further study for the economy reason.

4.1.2 The Effect of Drying Methods on BET Surface Area of $Ce_{0.75}Zr_{0.25}O_2$

$Ce_{0.75}Zr_{0.25}O_2$ catalysts were prepared by urea hydrolysis at 0.4M urea. Gel of $Ce_{0.75}Zr_{0.25}O_2$ was dried by two different methods. The gel that dried at conventional condition (100°C) is called xerogel whereas the gel that dried under the supercritical condition of ethanol (Pc=70bar, Tc=243°C) at 100 bar and 280°C would be called aerogel. As shown in Table 4.2, BET surface area, pore volumes and pore sizes of xerogel and aerogel for both calcine temperatures at 500°C and 900°C.

After calcination at 500°C, the BET surface area of xerogel and aerogel are similar, while pore volumes and pore sizes of aerogel are double when compare to those of xerogel, these results can be explained by the collapse of pore structure during drying. When gel was dried under conventional method (100°C), liquid trapped in the pore of gel is removed. As liquid evaporates, liquid-vapor interface develops inside a pore, and the accompanying surface tension pulls on the solid walls of the pore. The pore structure collapses during drying along with the differential capillary pressure that acts on pores of different sizes. In case of aerogel, the vapor-liquid interface disappears under supercritical conditions. Then, there is no surface tension to collapse the pores. Large pore volume and diameter of a solid can be maintained.

However, the surface area of aerogel and xerogel are different at calcined temperature of 900°C. Aerogel sample has higher BET surface area than that of xerogel. The explanation of these results can be trusted on the thermal stability of the catalyst. The drying under supercritical condition of ethanol enhances the thermal stability of $Ce_{0.75}Zr_{0.25}O_2$, resulting in better resistance to sintering and deactivation.

From the catalst testing study, xerogel has higher catalytic activity for iso-octane than aerogel. Thus, the catalyst dried at 100°C was chosen for the next part of studies.

Table 4.1 The effect of urea concentration on BET surface area of $Ce_{0.75}Zr_{0.25}O_2$ prepared with reaction time = 120 hours.

Calcine Temperature (°C)	BET Surface Area (m^2/g) of $Ce_{0.75}Zr_{0.25}O_2$		
	Urea Concentration		
	0.4M	1M	2M
500	104.5	122.9	132.9
900	14.43	28.12	13.86

Table 4.2 The effect of drying method on BET surface area of $Ce_{0.75}Zr_{0.25}O_2$ prepared with 0.4M urea and reaction time = 120 hours.

Calcine Temperature (°C)	BET Surface Area (m^2/g)		Pore Volume (cc/g)		Pore Size (nm)	
	Xerogel	Aerogel	Xerogel	Aerogel	Xerogel	Aerogel
500	104.5	104.6	0.0953	0.1804	3.58	6.90
900	14.43	31.37	0.0475	0.1014	13.70	12.93

4.1.3 The Effect of Ce and Zr Loading on BET Surface Area

The $Ce_{1-x}Zr_xO_2$ (x = 0, 0.25, 0.50, 0.75, 1.0) prepared by urea hydrolysis were measures the surface area by the multiple point BET method. Table 4.3 and Table 4.4 show the effect of Ce and Zr loading with different calcined temperatures and reaction times on the BET surface areas of catalysts.

The BET surface areas of $Ce_{1-x}Zr_xO_2$, calcined at both 500°C and 900°C, are higher than those of pure CeO_2 and ZrO_2 as can be seen in Table 4.1 and Table 4.2. The shape of individual particles can explain these results. The shapes of pure CeO_2 particles are mainly long

thin needle shape, while the shapes of pure ZrO_2 particles are flat and thick sheet. When CeO_2 was doped with ZrO_2, the long thin needle shape of CeO_2 will arrange to the spherical shape, resulting in a greater surface area.

In addition, the increase in the amount of ZrO_2 added in CeO_2 lattice increases the surface area of $Ce_{1-x}Zr_xO_2$. For example, BET surface area of $Ce_{0.25}Zr_{0.75}O_2$ (115.1 m^2/g) prepared with reaction time 50 hours and calcined at 500°C is higher than those of $Ce_{0.75}Zr_{0.25}O_2$ (104 m^2/g) and $Ce_{0.50}Zr_{0.50}O_2$ (109.6 m^2/g). The explanation of these results can be counted on thermal stability of the catalyst. The addition or incorporation of ZrO_2 to CeO_2 as a mixed oxide enhances thermal stability of CeO_2, resulting in better resistance of sintering and deactivation process. It is clear that CeO_2 undergoes a rapid crystalline growth process because BET surface area of pure CeO_2 with the reaction time 50 hours and 120 hours decrease significantly more than in the $Ce_{1-x}Zr_xO_2$. Consequently, the crystalline growth process is retarded or disordered by the addition and/or incorporation of ZrO_2 into CeO_2 lattice (Colon *et al.*, 1999)

Moreover, the surface area of $Ce_{1-x}Zr_xO_2$ is slightly effected by the reaction time. Table 4.1 and Table 4.2 show that the surface area of Ce/Zr mixed oxides prepared with reaction time 120 hours has higher BET surface area than those with reaction time 50 hours do. Because the arrangement of needle shapes to spherical shape was occurred in the function of the reaction time.

Table 4.3 BET surface area of catalysts prepared with the reaction time = 50 hours.

Calcine Temperature (°C)	BET Surface Area (m^2/g)				
	Ce:Zr				
	100:0	75:25	50:50	25:75	0:100
500	97.29	104	109.6	115.1	82.97
900	4.764	9.648	15.45	26.01	18.02

Table 4.4 BET surface area of catalysts prepared with the reaction time = 120 hours.

Calcine Temperature (°C)	BET Surface Area (m^2/g)				
	Ce:Zr				
	100:0	75:25	50:50	25:75	0:100
500	100.5	104.5	112.4	123.6	81.99
900	5.327	14.43	29.18	37.64	31.16

4.1.4 The Effect of Ni Loading on BET Surface Area

$Ce_{1-x}Zr_xO_2$ (x = 0.25, 0.50 and 0.75) were tested the catalytic activity for iso-octane oxidation. It is observed that $Ce_{0.75}Zr_{0.25}O_2$ has the highest catalytic activity for iso-octane oxidation. Thus, 5% of Ni was loaded on $Ce_{0.75}Zr_{0.25}O_2$.

Table 4.5 shows the effect of Ni loading on the BET surface area of catalysts at both calcined temperatures 500°C and 900°C. $Ce_{0.75}Zr_{0.25}O_2$ was prepared with 0.4M of urea at reaction time 120 hours. The obtained gel was loaded with Ni and dried at 100°C. After calcination at 500°C, the addition of Ni decreases the BET surface area of

$Ce_{0.75}Zr_{0.25}O_2$. The lost of surface area was due to the interaction between Ni and the support. However, the 5%Ni/$Ce_{0.75}Zr_{0.25}O_2$ has higher BET surface area than the unloaded $Ce_{0.75}Zr_{0.25}O_2$ at calcined temperature 900°C. It is suggesting that thermal stability of $Ce_{0.75}Zr_{0.25}O_2$ be improved by the addition of Ni.

Table 4.5 The effect of Ni loading on BET surface area of $Ce_{0.75}Zr_{0.25}O_2$ prepared with 0.4M urea and reaction time = 120 hours.

Calcine Temperature (°C)	BET Surface Area (m^2/g)	
	$Ce_{0.75}Zr_{0.25}O_2$	5%Ni/$Ce_{0.75}Zr_{0.25}O_2$
500	104.50	70.50
900	14.43	17.30

4.2 X-Ray Diffraction (XRD)

4.2.1 The XRD Patterns of $Ce_{1-x}Zr_xO_2$

The XRD patterns of samples with different Ce and Zr loading are given in Figures 4.1 and 4.2 for the samples calcined at 500°C and Figure 4.3 and Figure 4.4 for the samples calcined at 900°C with varying reaction times.

CeO_2 has the fluorite (CaF_2) structure made of a close-packed cubic array of metal atoms in which all tetrahedral holes are filled by oxygen (Travarelli *et al.*, 1997). This structure can be represented by the XRD spectrum corresponding to the (111), (200), (200), (311), (222) and (400) planes (at about 29°, 33°, 48°, 56°, 60° and 70°, (2θ)) as shown in Figure 4.1, 4.2, 4.3 and 4.4.

The XRD patterns of $Ce_{1-x}Zr_xO_2$ catalyst (x = 0, 0.25, 0.50, 0.75 and 1.0) calcined at 500°C shown in Figure 4.1 and 4.2 can be divided into two groups. They are the XRD patterns of $Ce_{0.75}Zr_{0.25}O_2$ and the XRD patterns of $Ce_{0.50}Zr_{0.50}O_2$.

The XRD pattern of $Ce_{0.75}Zr_{0.25}O_2$ is consistent with that of CeO_2. The XRD pattern exhibits the six main reflections typical of a cubic fluorite-structured material with a fcc cell, corresponding to the (111), (200), (200), (311), (222) and (400) planes (at about 29°, 33°, 48°, 56°, 60° and 70°, (2θ)).

For the XRD pattern of $Ce_{0.50}Zr_{0.50}O_2$, the six main reflections typical of a fluorite-structured material with a fcc cell were observed. However, there is some tetragonality of the obtained phase as indicated by the splitting of the (111), (200) and (220) reflection at about 30°, 35° and 50° (2θ), respectively.

$Ce_{1-x}Zr_xO_2$ preferably crystallizes into a cubic phase, if x is equal or lower than 0.50, whereas a tetragonal cell is favored for x is higher than 0.50 (Figure 4.1 and Figure 4.2).

As shown in Figure 4.1 and Figure 4.2, no peak of ZrO_2 was found in any XRD patterns of $Ce_{1-x}Zr_xO_2$ (x = 0.25, 0.50 and 0.75). It is suggesting that Zr was incorporated into the CeO_2 lattice to form a solid solution while maintain the fluorite structure.

Figures 4.3 and 4.4 show the XRD patterns of $Ce_{1-x}Zr_xO_2$ with the reaction time equal to 50 hours and 120 hours and calcined at 900°C. All peaks of $Ce_{1-x}Zr_xO_2$ have the same position as those calcined at 500°C. The peak intensity of the sample calcined at 900°C, however, is higher than that of sample calcined at 500°C. Moreover, the width of the XRD peaks of the sample calcined at 900°C is narrower than those calcined at 500°C, suggesting an increase in particle size due to the sample sintering (Christine et al., 2000).

The XRD patterns shown in Figure 4.3 and Figure 4.4 can also be grouped into two patterns; the XRD pattern of $Ce_{0.75}Zr_{0.25}O_2$ that is similar to that of CeO_2 alone and the XRD pattern of $Ce_{0.50}Zr_{0.50}O_2$.

The XRD pattern of $Ce_{0.75}Zr_{0.25}O_2$ exhibits the six main reflections belong to a cubic fluorite-structured phase with an fcc cell, corresponding to the (111), (200), (200), (311), (222) and (400) planes (at about 29°, 33°, 48°, 56°, 60° and 70°, (2θ)). This pattern is consistent with that of CeO_2.

For the XRD pattern of $Ce_{0.50}Zr_{0.50}O_2$, these six main reflections typical of a fluorite-structured material with a fcc cell are also observed. However, tetragonal phase was indicated by the splitting of the (111), (200) and (220) reflection at about 30°, 35° and 50° (2θ), respectively.

After calcination at 900°C, the $Ce_{1-x}Zr_xO_2$ sample preferably crystallizes into a cubic phase, if x is equal or lower than 0.50, whereas a

tetragonal cell is favored for x is higher than 0.50. In addition, a monoclinic phase is performed in the sample with high ZrO_2 content.

As shown in Figure 4.3 and Figures 4.4, there is no peak typical of free ZrO_2 observed in the XRD patterns of $Ce_{1-x}Zr_xO_2$ (x = 0.25, 0.50 and 0.75) after calcination at 900°C. Thus, it is suggesting that ZrO_2 is incorporated into CeO_2 lattice to form a solid solution while maintain the fluorite-structure.

As compare with the XRD spectrum of CeO_2, the XRD peaks that observed for $Ce_{1-x}Zr_xO_2$ solid solution became broader. This broadening could be ascribed to the distortion of cubic phase of fluorite structure to a tetragonal one. This occurrence was due to the incorporation of Zr into CeO_2.

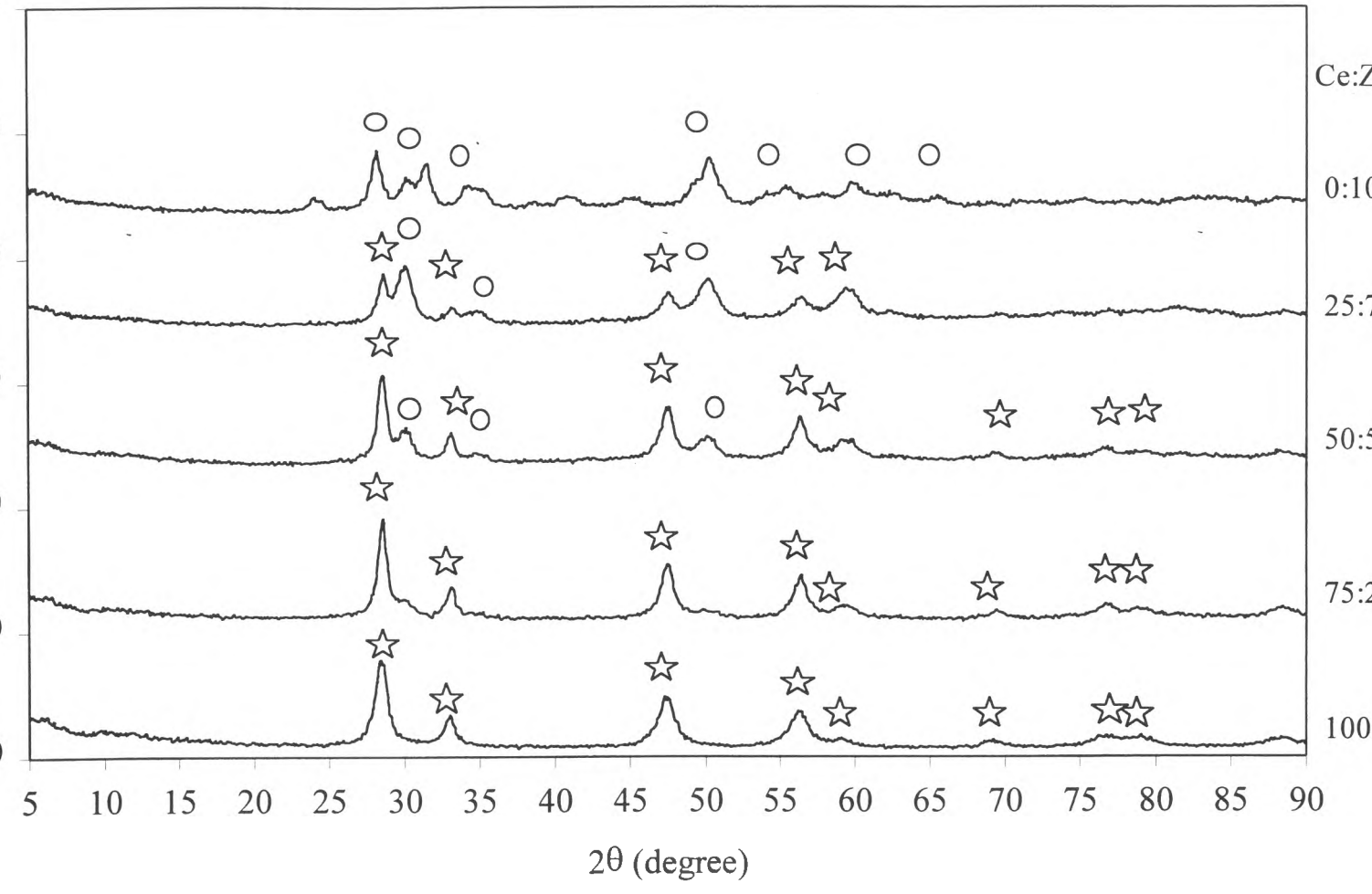

XRD patterns of $Ce_{1-x}Zr_xO_2$ with the reaction time equal to 50 hours and calcined at 500°C; (O) tet
cubic phase.

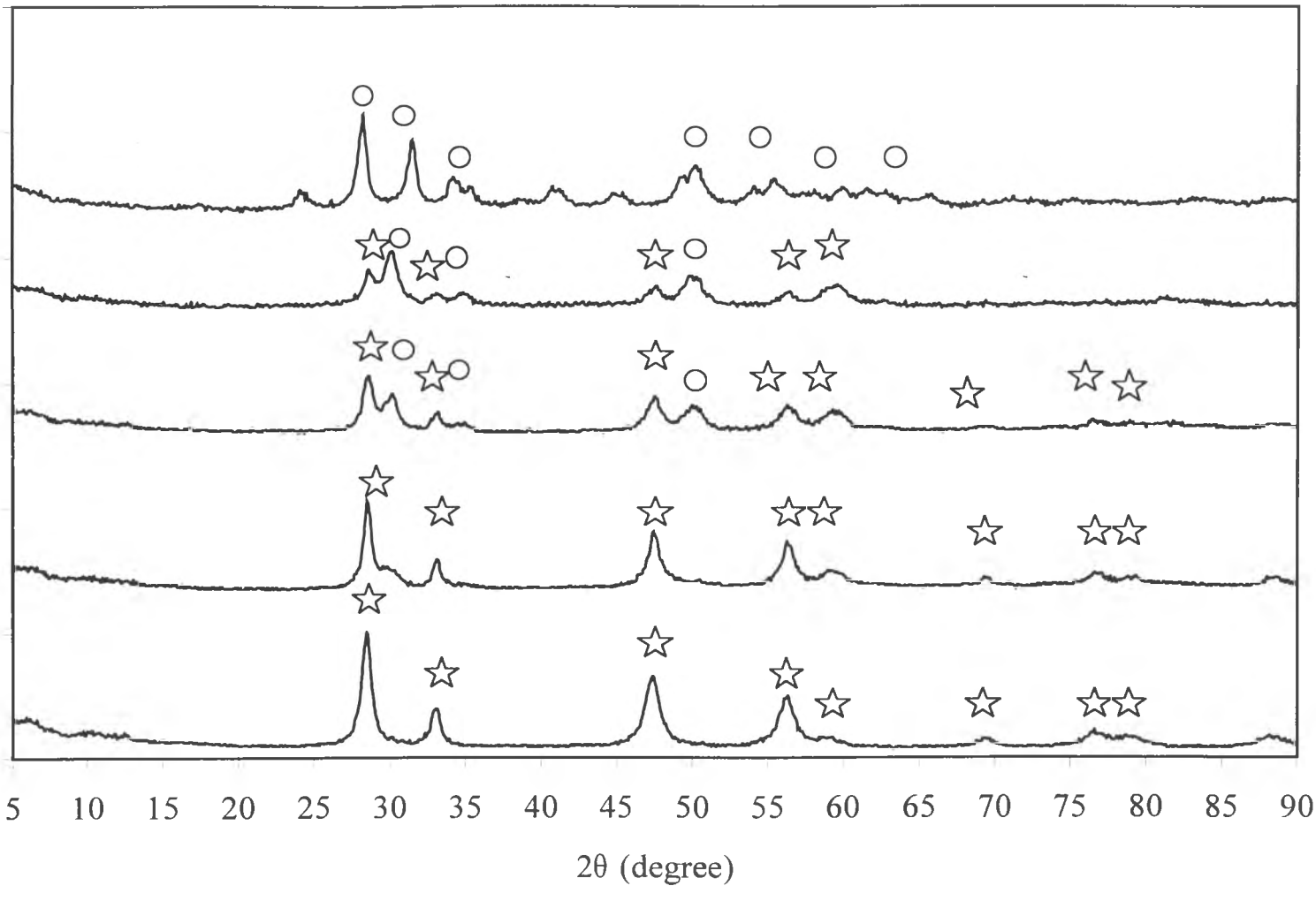

XRD patterns of $Ce_{1-x}Zr_xO_2$ with the reaction time equal to 120 hours and calcined at 500°C; (O) tetragona
hase.

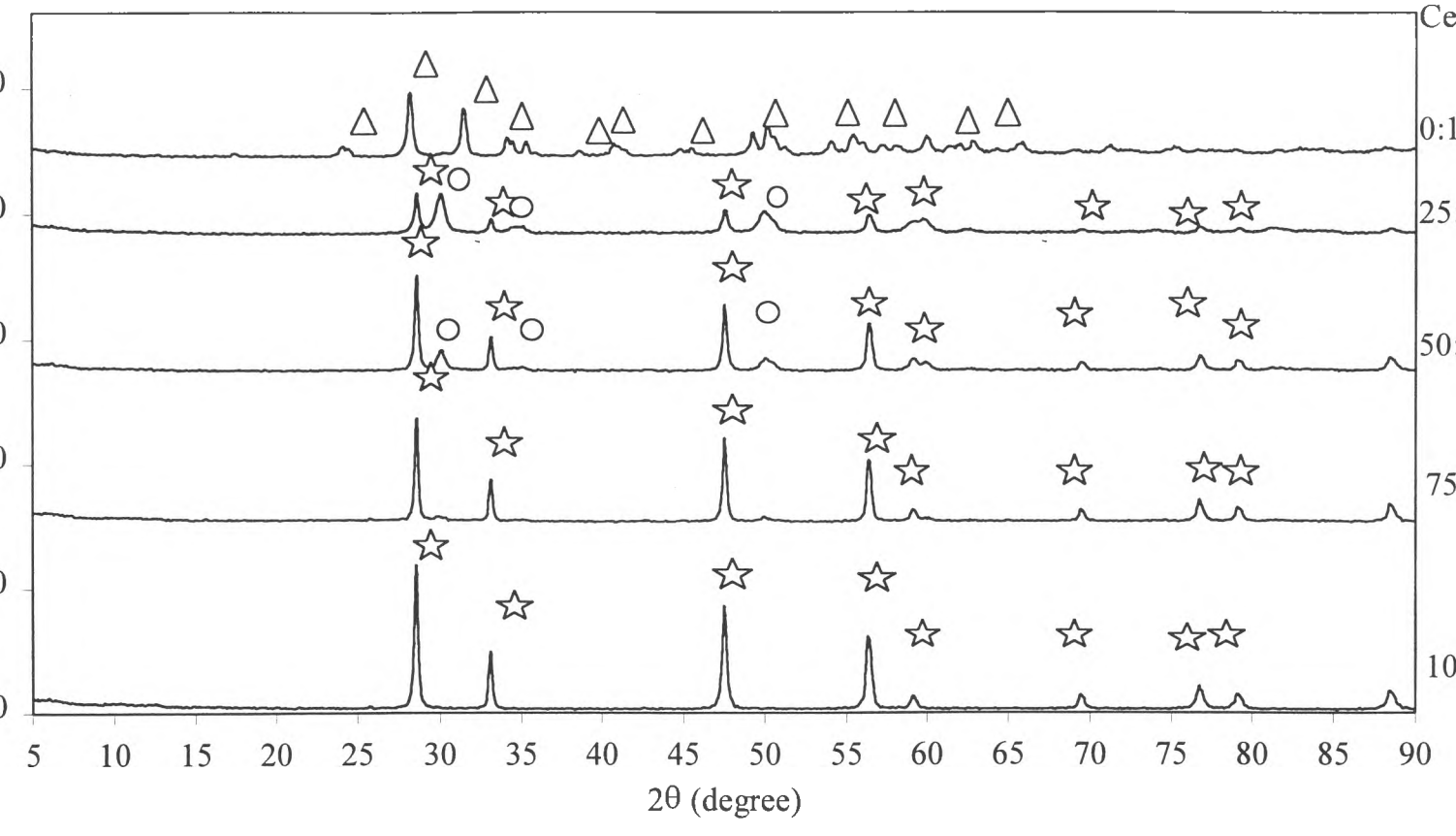

XRD patterns of $Ce_{1-x}Zr_xO_2$ with the reaction time equal to 50 hours and calcined at 900°C; (O) tet
cubic phase, (Δ) monoclinic phase.

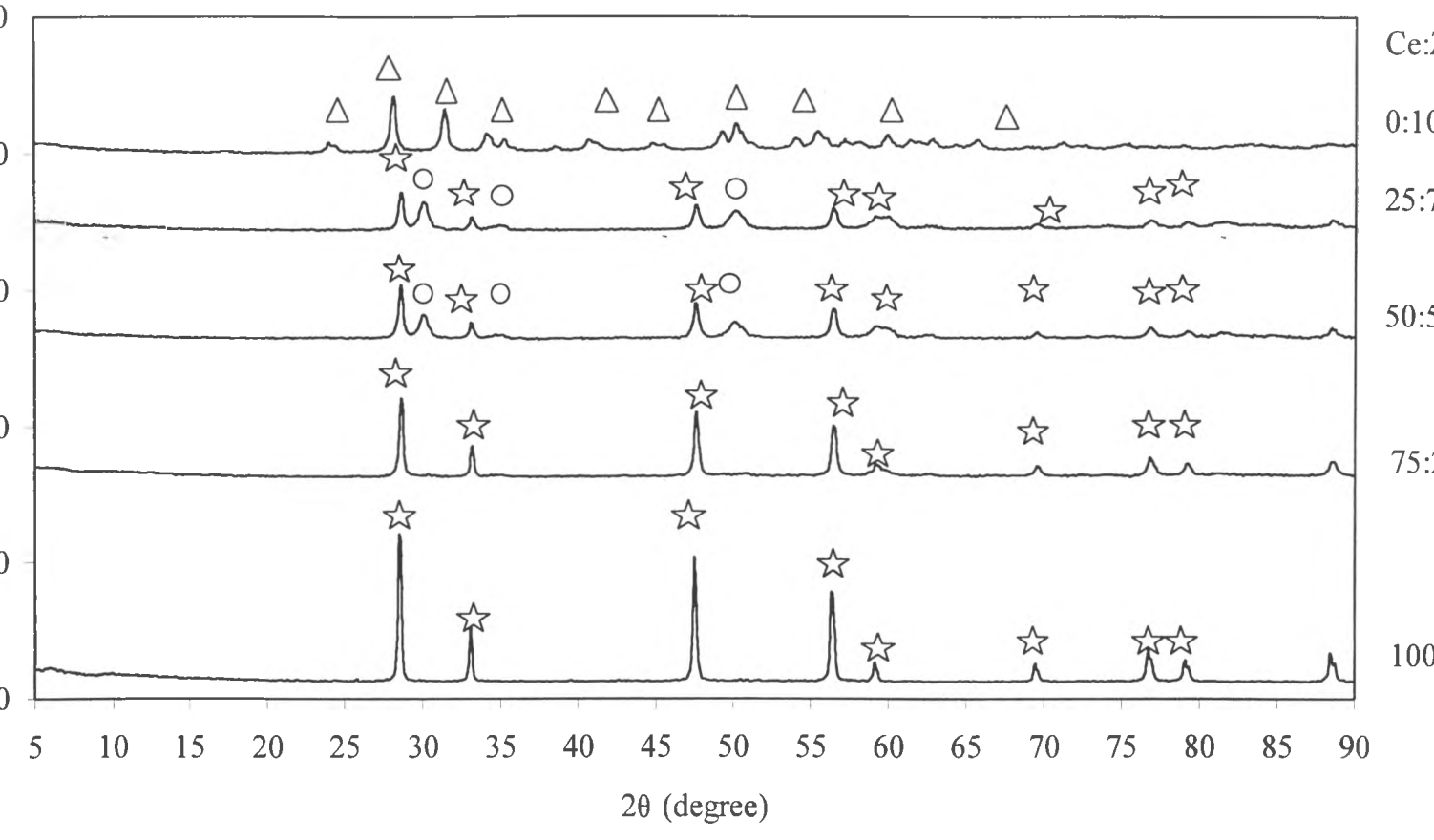

4 XRD patterns of $Ce_{1-x}Zr_xO_2$ with the reaction time equal to 120 hours and calcined at 900°C; (O) tet
cubic phase, (Δ) monoclinic phase.

4.2.2 The XRD Patterns of $Ce_{0.75}Zr_{0.25}O_2$ Prepared with Different Urea Concentrations

Figure 4.5 and Figure 4.6 show the XRD patterns of $Ce_{0.75}Zr_{0.25}O_2$ prepared by urea hydrolysis with different urea concentrations at reaction time equal to 120 hours and calcined at 500°C and 900°C.

All XRD patterns of $Ce_{0.75}Zr_{0.25}O_2$ prepared with 0.4M, 1M and 2M urea and calcined at 500°C exhibit the cubic fluorite-structured material with a fcc cell. These patterns are composed of six peaks corresponding to the (111), (200), (200), (311), (222) and (400) planes (at about 29°, 33°, 48°, 56°, 60° and 70°, (2θ)), which are consistent with that of CeO_2. After calcination at 900°C, the tetragonal phase detected by the splitting of the (111) and (220) reflection at about 30° and 50° (2θ) was observed in of $Ce_{0.75}Zr_{0.25}O_2$ prepared with 1M and 2M urea.

The peak intensity was decreases with the increase in urea concentrations. This resulted from the different degree of porosity and crystallinity of $Ce_{0.75}Zr_{0.25}O_2$ prepared with various urea concentrations. It is found that urea concentration does not effect on the structure of the catalyst.

There is no observation of ZrO_2 peaks in any the XRD patterns of $Ce_{0.75}Zr_{0.25}O_2$ prepared with different urea concentrations, suggesting that Zr is incorporated into CeO_2.

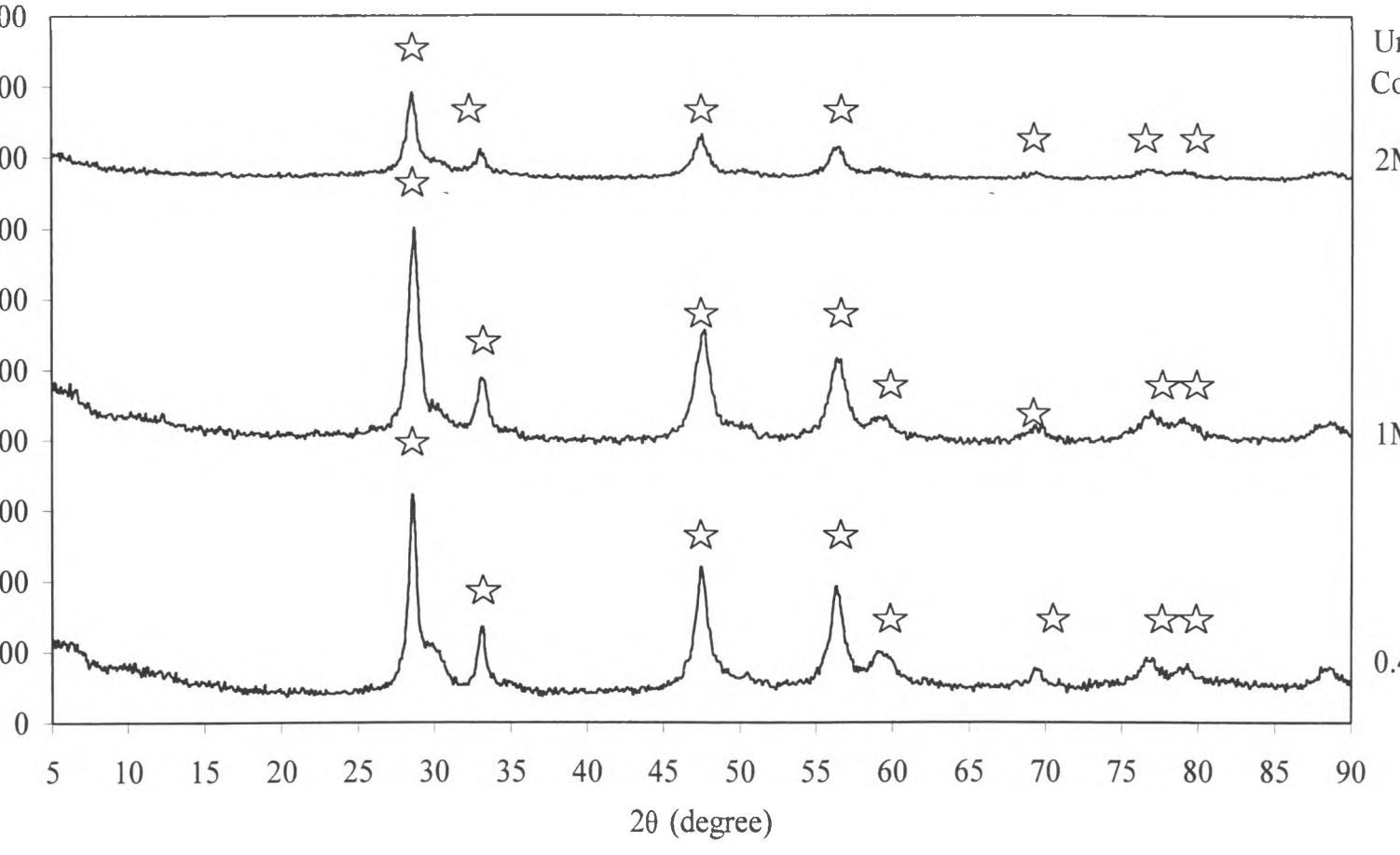

XRD patterns of $Ce_{0.75}Zr_{0.25}O_2$ prepared with different urea concentrations, the reaction time equal to 12
d at 500°C; (☆) cubic phase.

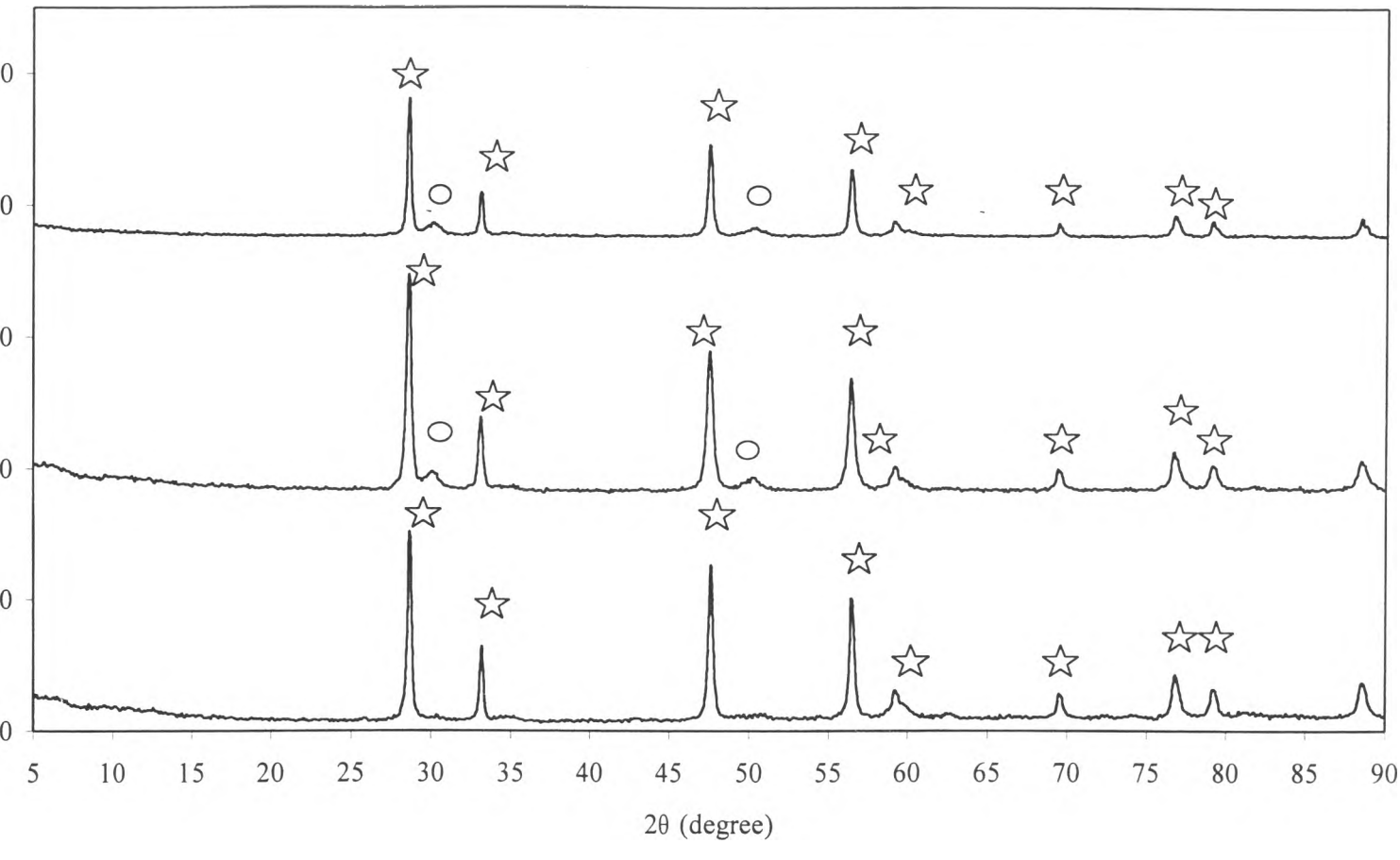

5 XRD patterns of $Ce_{0.75}Zr_{0.25}O_2$ with different urea concentrations, the reaction time equal to 120 ho
900°C; (O) tetragonal phase, (☆) cubic phase.

4.2.3 The XRD Patterns of $Ce_{0.75}Zr_{0.25}O_2$ Prepared with Different Drying Methods

Figure 4.7 and Figure 4.8 display the XRD patterns of $Ce_{0.75}Zr_{0.25}O_2$ prepared with different drying method at reaction time 120 hours and calcined at 500°C and 900°C. The xerogel sample is $Ce_{0.75}Zr_{0.25}O_2$ dried at 100°C, and the aerogel sample is $Ce_{0.75}Zr_{0.25}O_2$ dried under the supercritical condition of ethanol ((Pc=70bar, Tc=243°C) at 100 bar and 280°C.

As can be seen in Figure 4.7, the aerogel sample calcined at 500°C, has similar XRD pattern to that of xerogel sample. The XRD peaks corresponding to the (111), (200), (200), (311), (222) and (400) planes (at about 29°, 33°, 48°, 56°, 60° and 70°, (2θ)) indicate the cubic fluorite-structured with a fcc cell, which consistent with the XRD pattern of pure CeO_2.

The XRD patterns of both xerogel and aerogel calcined at 900°C are very similar (Figure 4.8). The XRD patterns of both samples index the fluorite-structured with an fcc cell. In addition, the tetragonal phase is observed in the XRD pattern of the aerogel of $Ce_{0.75}Zr_{0.25}O_2$ by the splitting of the (111) and (220) reflection at about 30° and 50° (2θ), respectively.

From Figure 4.8, the difference in the peak intensity is due to the sample sintering. The BET surface area can insist this occurrence. After calcination at 900°C, the aerogel has higher BET surface area than the xerogel's. It can be concluded that the drying under super critical condition enhances thermal stability of $Ce_{0.75}Zr_{0.25}O_2$ catalyst.

There was no free ZrO_2 detected in any the XRD patterns of $Ce_{0.75}Zr_{0.25}O_2$ prepared with different drying methods, suggesting that Zr is incorporated into CeO_2.

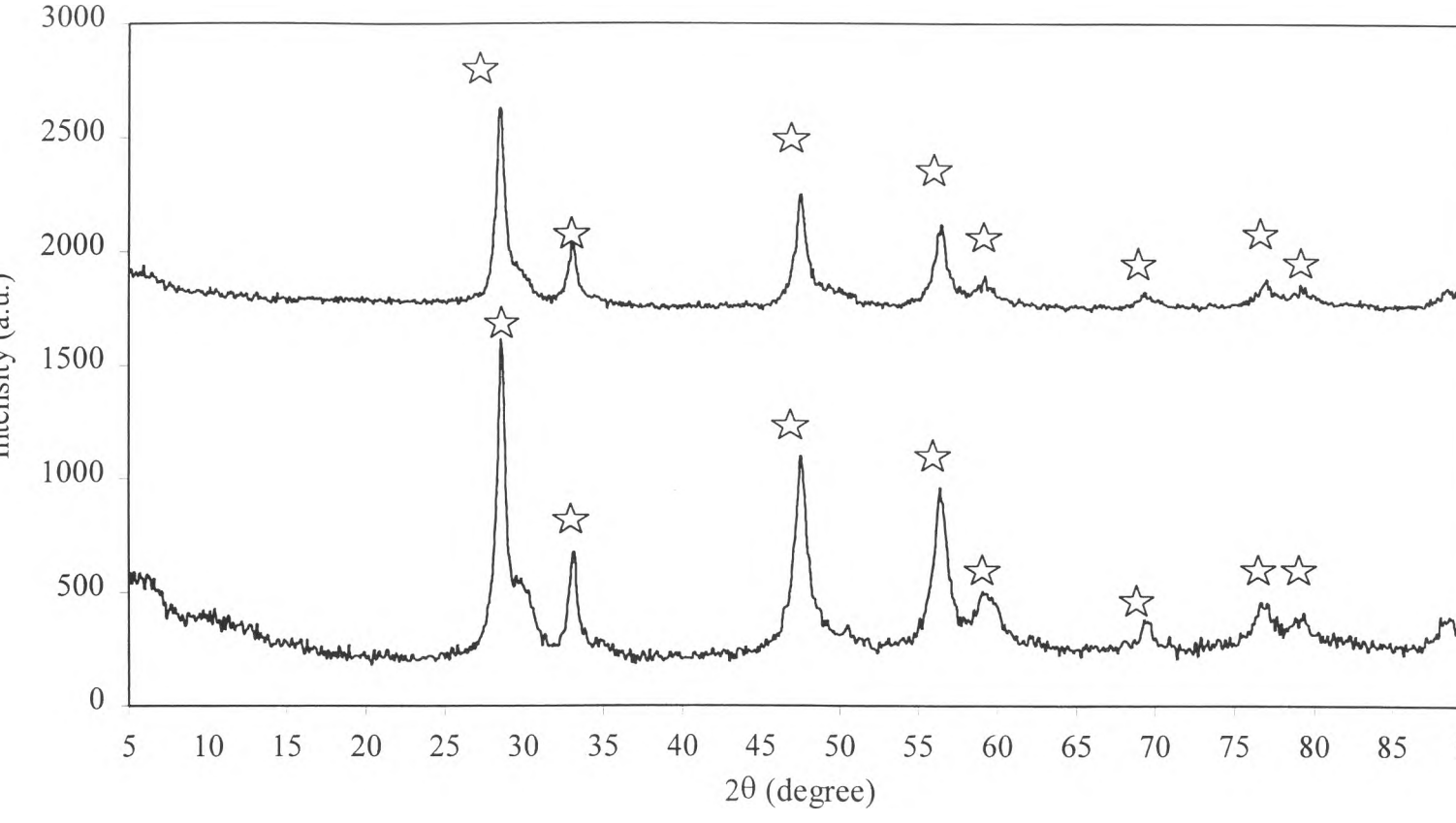

ure 4.7 XRD patterns of xerogel and aerogel of $Ce_{0.75}Zr_{0.25}O_2$ with the reaction time equal to 120 hou
00°C; (☆) cubic phase.

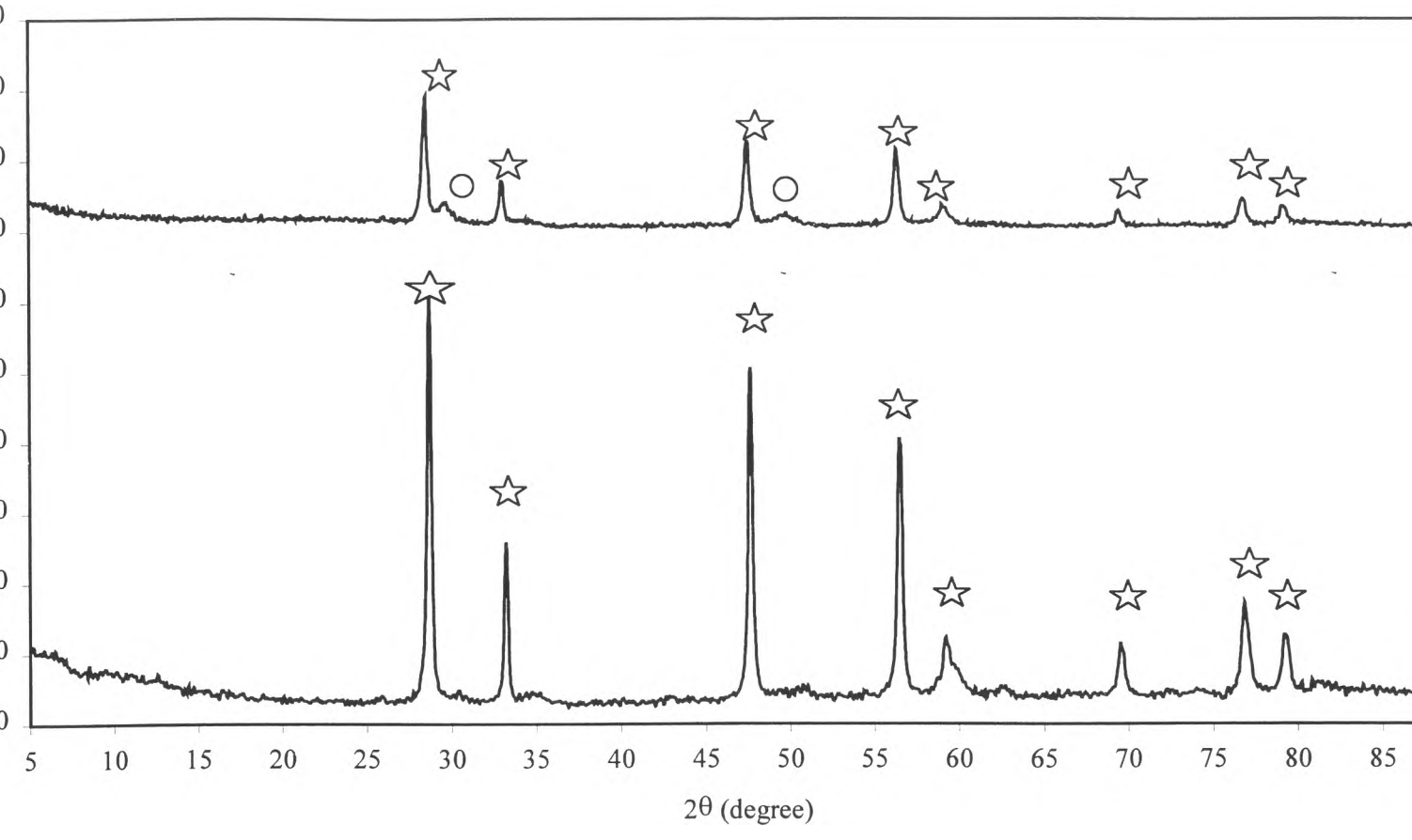

8 XRD patterns of xerogel and aerogel of $Ce_{0.75}Zr_{0.25}O_2$ with the reaction time equal to 120 hours
) tetragonal phase, (☆) cubic phase.

4.2.4 The XRD Patterns of 5%Ni/$Ce_{0.75}Zr_{0.25}O_2$

The comparison of the XRD patterns of 5%Ni/$Ce_{0.75}Zr_{0.25}O_2$ and $Ce_{0.75}Zr_{0.25}O_2$ with reaction time are shown in Figure 4.9 and Figure 4.10 for the samples calcined at 500°C and 900°C.

The XRD patterns of both samples, calcined at 500°C and 900°C, exhibits the six main reflections typical of a fluorite-structured material with a fcc cell, corresponding to the (111), (200), (200), (311), (222) and (400) planes (at about 29°, 33°, 48°, 56°, 60° and 70°, (2θ)). This pattern is consistent with that of CeO_2.

As shown in Figure 4.9 and Figure 4.10, all peaks of the XRD spectra of $Ce_{0.75}Zr_{0.25}O_2$ have higher intensity than those of 5%Ni/$Ce_{0.75}Zr_{0.25}O_2$. This occurrence was due to the increase particle size due to the sample sintering. Thus, the addition of Ni can improve the thermal stability of $Ce_{0.75}Zr_{0.25}O_2$ catalyst. However, There is no NiO was observed in the XRD spectra of 5%Ni/$Ce_{0.75}Zr_{0.25}O_2$, suggesting that Ni is highly dispersed on $Ce_{0.75}Zr_{0.25}O_2$.

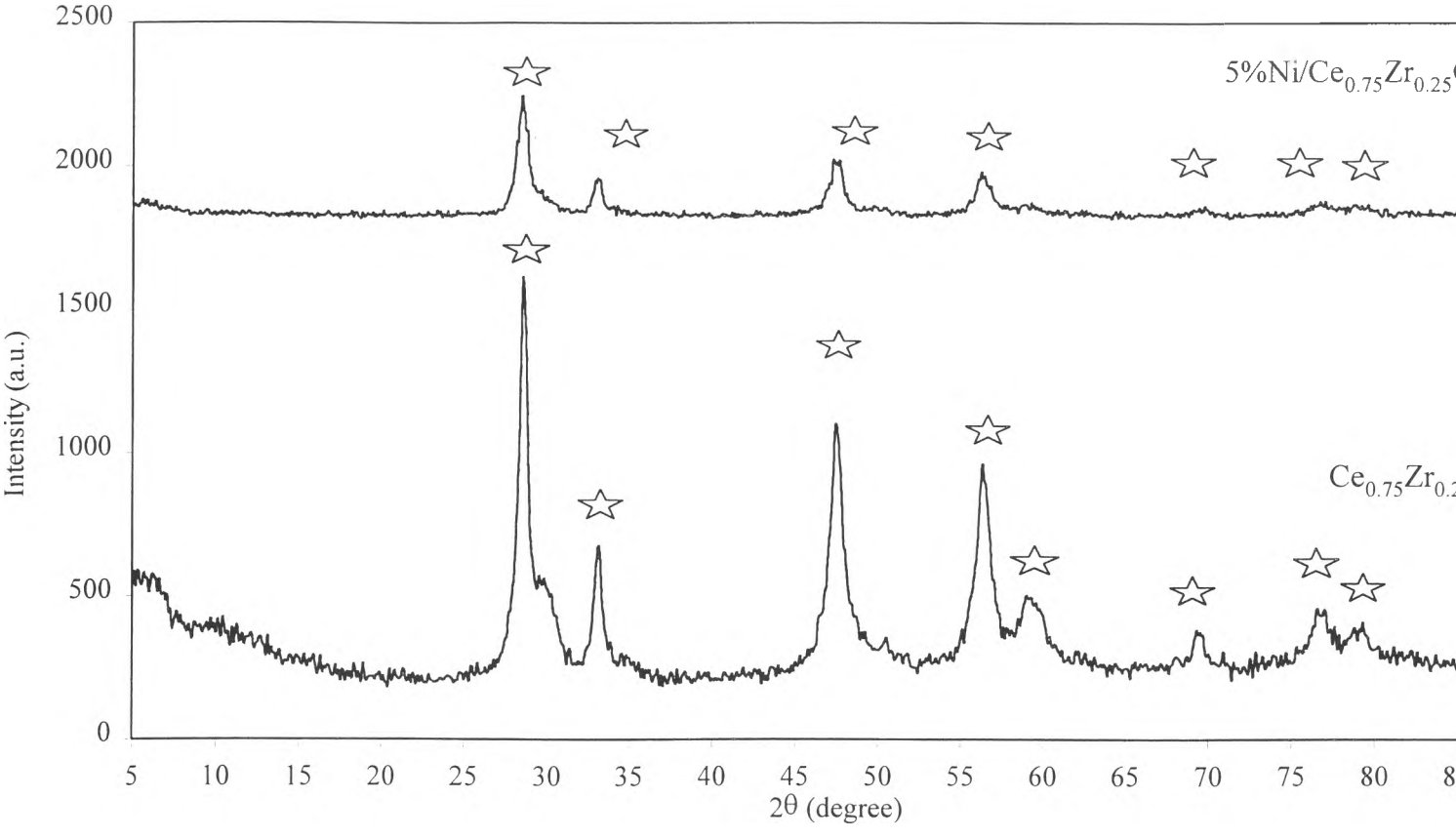

ure 4.9 XRD patterns of 5%Ni/$Ce_{0.75}Zr_{0.25}O_2$ with the reaction time equal to 120 hours and calcined

ic phase.

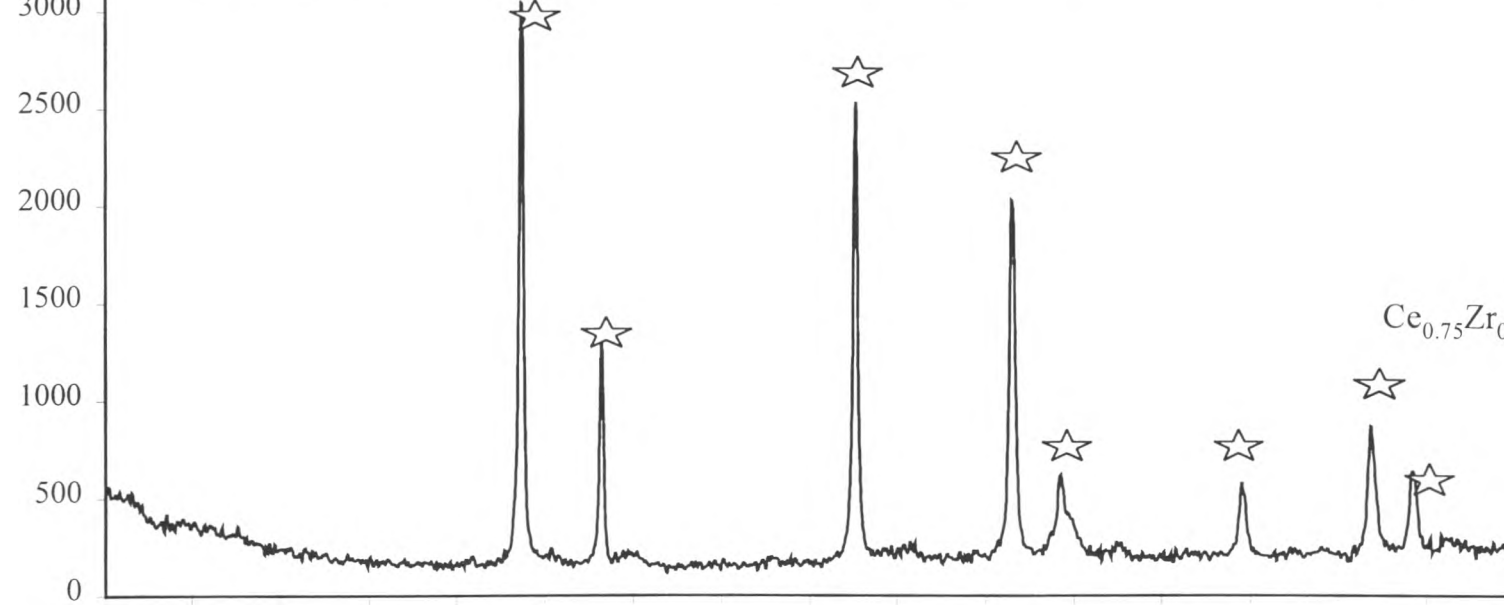
3000
2500
2000
1500
1000
500
0
$Ce_{0.75}Zr_{0}$

4.3 FT-Raman Spectroscopy

4.3.1 The FT-Raman of $Ce_{1-x}Zr_xO_2$

Figure 4.11 to Figure 4.14 exhibit the FT-Raman spectra of $Ce_{1-x}Zr_xO_2$ catalyst (x = 0, 0.25, 0.50, 0.75 and 1.0) with varying reaction time in the wavelength 400 to 900 cm^{-1}.

The summary of the FT-Raman results are reported in Table 4.6 for $Ce_{1-x}Zr_xO_2$ calcined at 500°C, and Table 4.7 for the sample calcined at 900°C.

Table 4.6 Raman Shift of strong peaks of FT-Raman spectra of $Ce_{1-x}Zr_xO_2$ catalyst calcined at 500°C.

Reaction time (hr)	Raman shift (cm^{-1})				
	Ce:Zr Ratio				
	100:0	75:25	50:50	25:75	0:100
50	465	464	465	465	-
120	463	463	463	463	-

Table 4.7 Raman Shift of strong peaks of FT-Raman spectra of $Ce_{1-x}Zr_xO_2$ catalyst calcined at 900°C.

Reaction time (hr)	Raman shift (cm^{-1})				
	Ce:Zr Ratio				
	100:0	75:25	50:50	25:75	0:100
50	466	466	466	466	-
120	465	466	465	466	-

The Raman spectra of $Ce_{1-x}Zr_xO_2$ with reaction time 50 hours and 120 hours are very similar. The spectrum of those calcined at 500°C feature a strong peak at about 465 cm^{-1} as can be seen in Figure 4.11 and Figure 4.12. The peak at 465 cm^{-1} is characteristic of the F_{2g} Raman active of a fluorite-structured. The patterns suggested some distortion of the oxygen lattice, which is consistent with the presence of cubic phases.

Figure 4.13 and 4.14 show the Raman spectra of $Ce_{1-x}Zr_xO_2$ calcined at 900°C that is similar to the Raman spectra of those of calcined at 500°C as shown in Figure 4.11 and 4.12. The spectrum of those calcined at 900°C also feature a strong peak at about 465 cm^{-1}, which is typical of the F_{2g} Raman active of a fluorite-structured. The peak intensity of the Raman spectra of those calcined at 900°C, however, is higher than those calcined at 500°C. This is consistent with sample sintering. The different intensity of the peaks in the samples may originate from the different degree of porosity and crystallinity of the catalyst. No peak of free ZrO_2 were detected, indicating that Zr was incorporated into CeO_2.

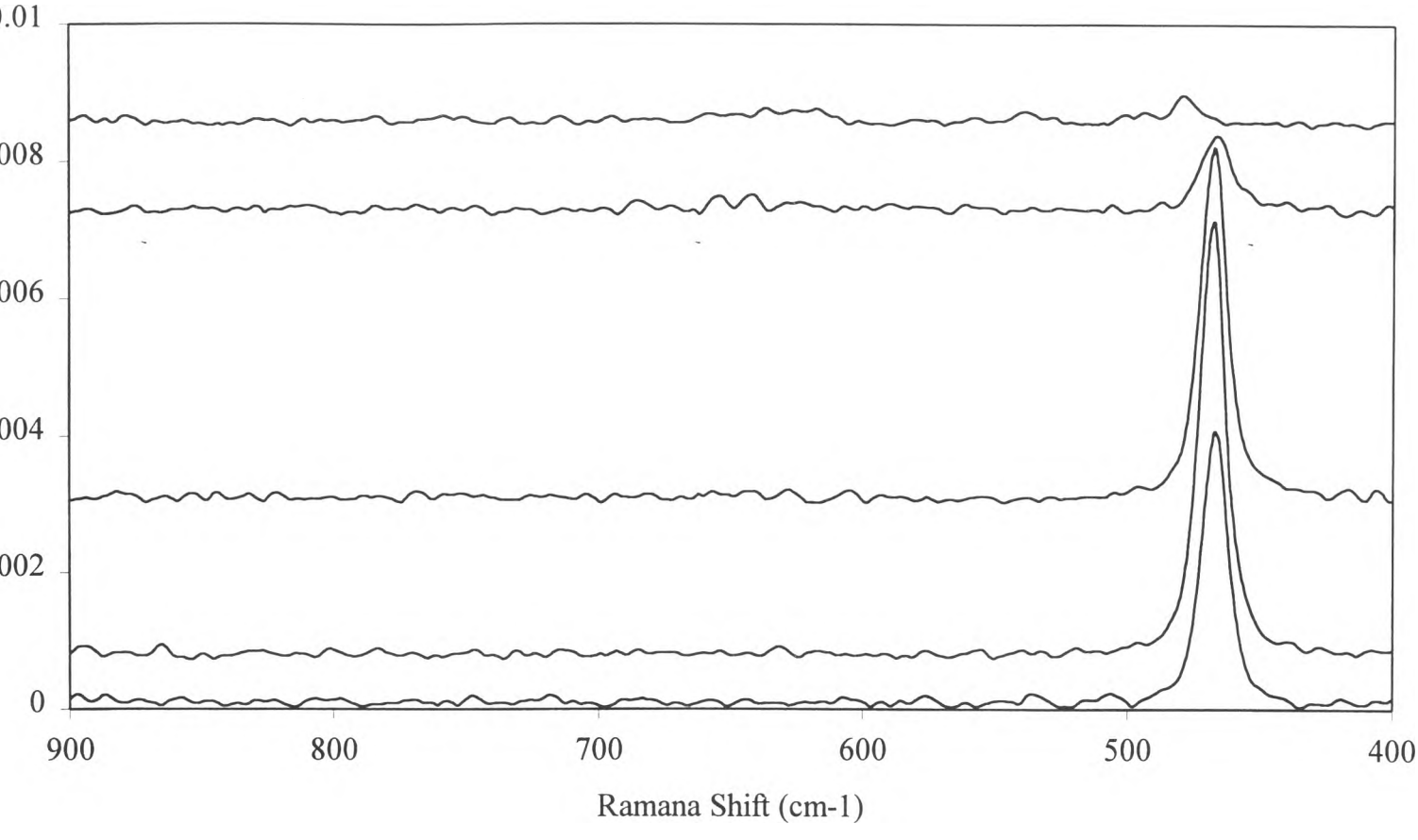

Figure 4.11 FT-Raman Spectra of $Ce_{1-x}Zr_xO_2$ with the reaction time equal to 50 hours and calcined at 500°C

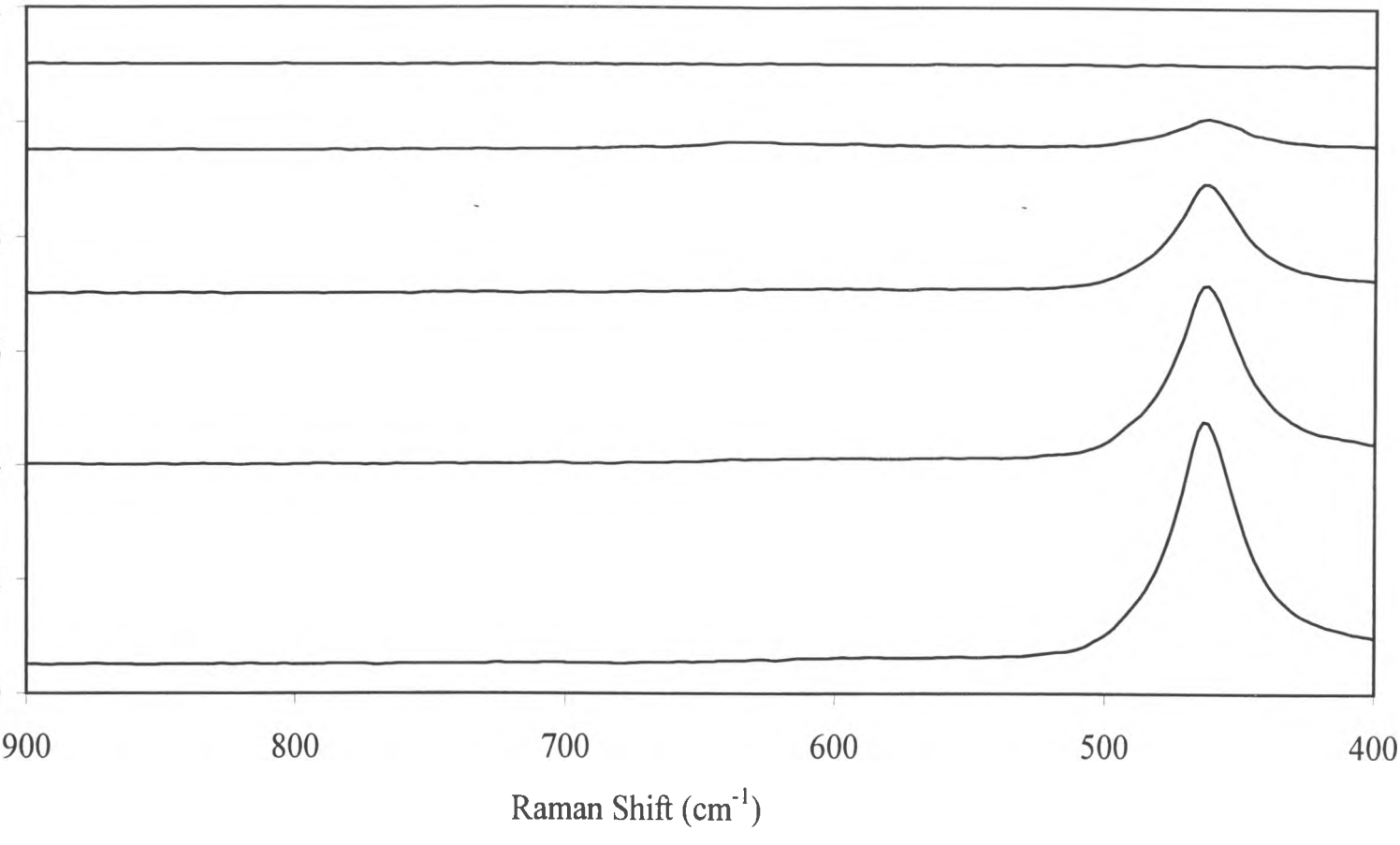

Figure 4.12 FT-Raman Spectra of $Ce_{1-x}Zr_xO_2$ with the reaction time equal to 120 hours and calcined at 500°C

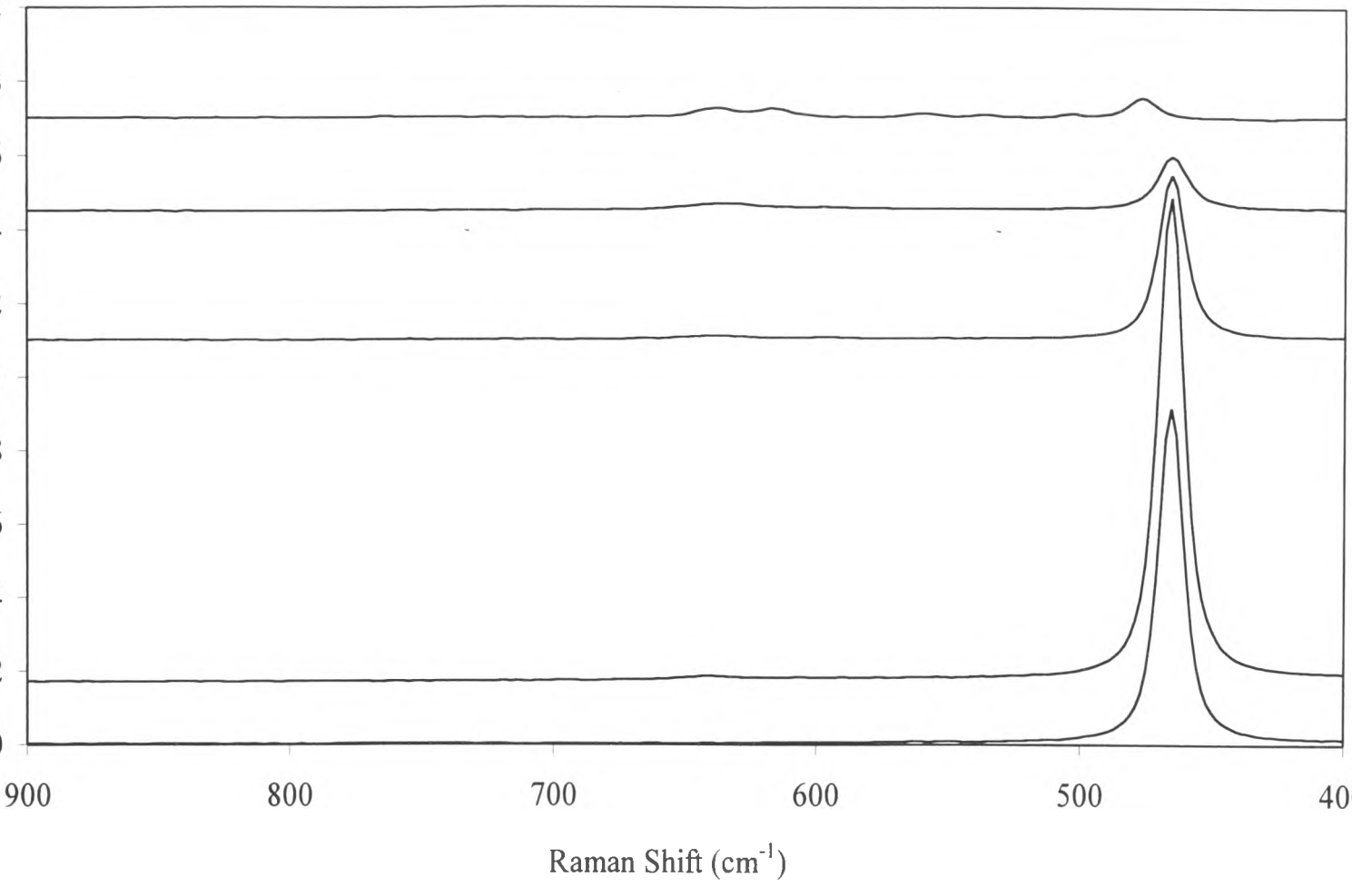

Figure 4.13 FT-Raman Spectra of $Ce_{1-x}Zr_xO_2$ with the reaction time equal to 50 hours and calcined at 900°C

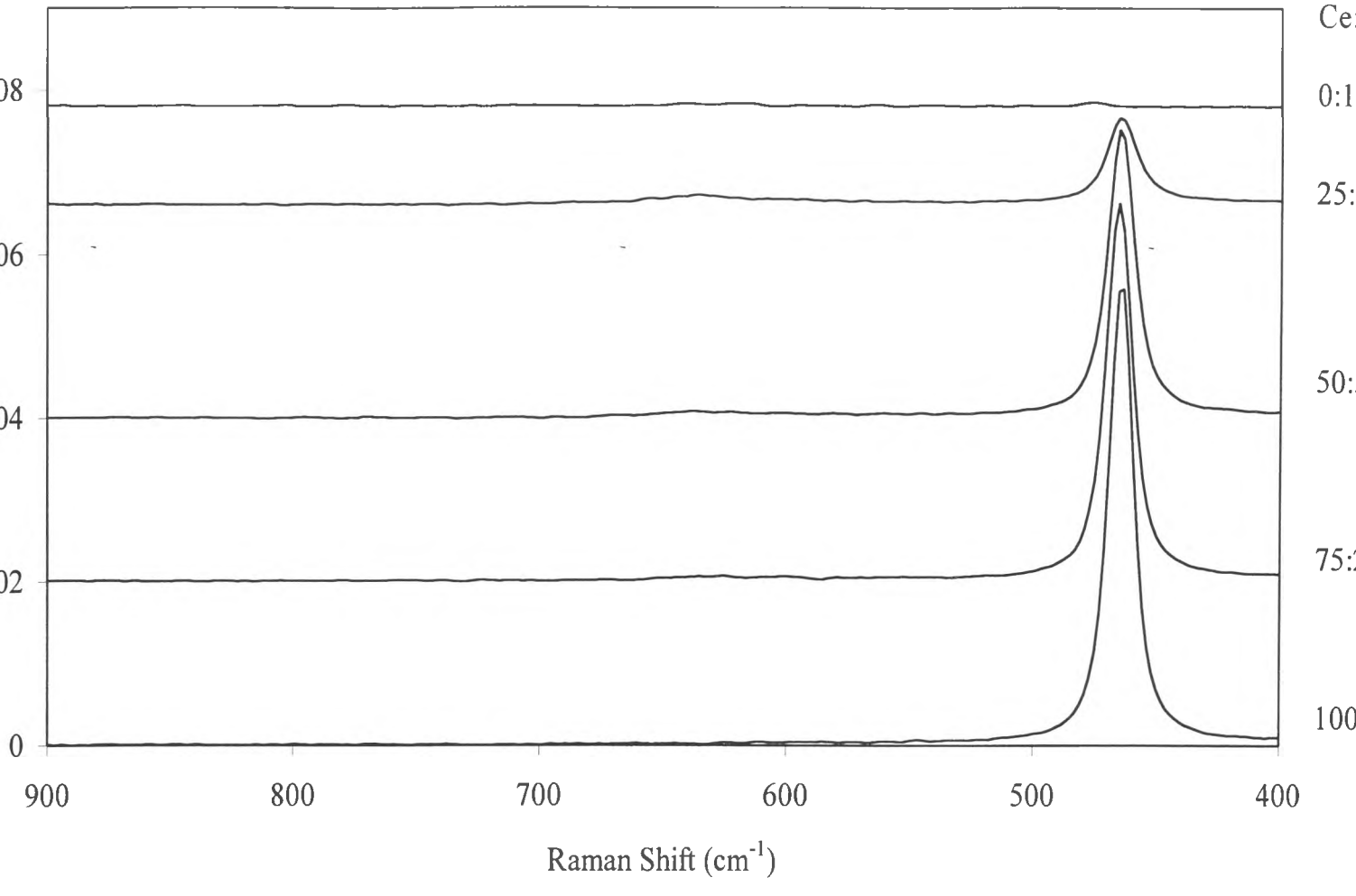

Figure 4.14 FT-Raman Spectra of $Ce_{1-x}Zr_xO_2$ with the reaction time equal to 120 hours and calcined at 900°C

4.3.2 The FT-Raman Spectra of $Ce_{0.75}Zr_{0.25}O_2$ Prepared Different Urea Concentrations

Figure 4.15 to figure 4.16 shows the FT-Raman spectra of $Ce_{0.75}Zr_{0.25}O_2$ catalyst prepared with varying urea concentration in the wavelength 400 to 900 cm^{-1}. Table 4.8 shows the summary of the FT-Raman results for the samples calcined at 500°C and 900°C.

As can be seen in Figure 4.15 and Figure 4.16, the FT-Raman spectra of $Ce_{0.75}Zr_{0.25}O_2$ catalyst with 0.4M, 1M and 2M of urea are very similar. The spectrum at about 465 cm^{-1} representative of the cubic fluorite-structured in the F_{2g} Raman active mode. The different peak intensity was resulted from the different degree of porosity and crystallinity.

Table 4.8 Raman Shift of strong peaks of FT-Raman spectra of $Ce_{0.75}Zr_{0.25}O_2$ prepared by various urea concentrations.

Calcine temperature (°C)	**Raman shift (cm^{-1})**		
	Urea concentration		
	0.4 M	**1 M**	**2 M**
500	463	462	462
900	465	466	466

4.3.3 The FT-Raman Spectra of $Ce_{0.75}Zr_{0.25}O_2$ Prepared Different Drying Methods

Figure 4.17 to figure 4.18 shows the FT-Raman spectra of $Ce_{0.75}Zr_{0.25}O_2$ catalyst with varying drying methods in the wavelength 400 to 900 cm^{-1}. Table 4.9 exhibits the summary of the FT-Raman results for the samples calcined at 500°C and 900°C.

The Raman spectra of the aerogel and xerogel are very similar as shown in Figure 4.17 to figure 4.18. The Raman spectrum typical of the F_{2g} Raman active mode of a fluorite-structured is observed at the peak about about 465 cm^{-1}. The difference of peak intensity indicated the difference in crystallize size due to the sample sintering.

Table 4.9 Raman Shift of strong peaks of FT-Raman spectra of $Ce_{0.75}Zr_{0.25}O_2$ prepared by different urea concentration.

Calcine temperature (°C)	**Raman shift (cm^{-1})**	
	Drying method	
	xerogel	**aerogel**
500	463	465
900	465	465

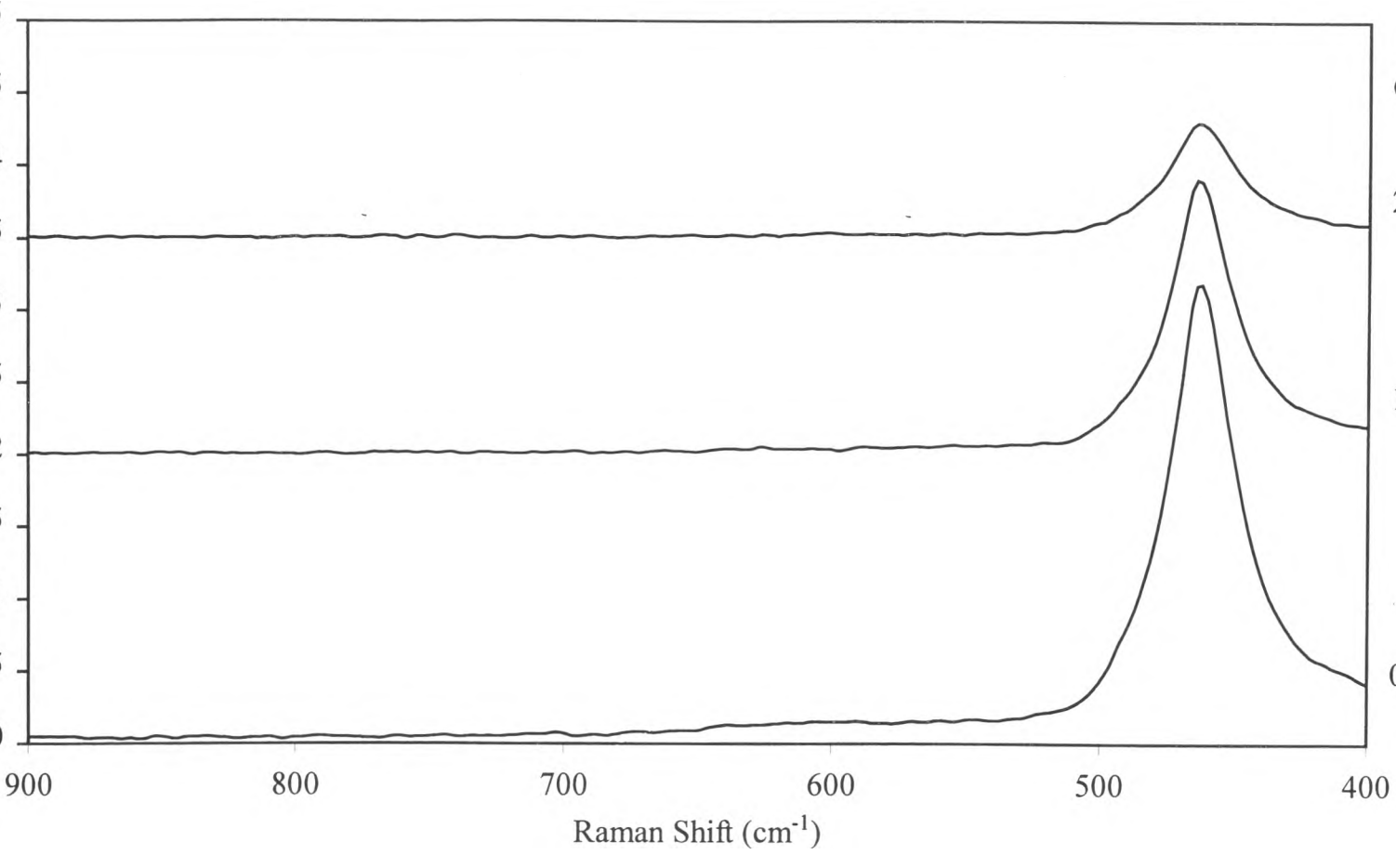

Figure 4.15 FT-Raman Spectra of $Ce_{0.75}Zr_{0.25}O_2$ prepared with different urea concentrations, the reactio time equal to 120 hours and calcined at 500°C

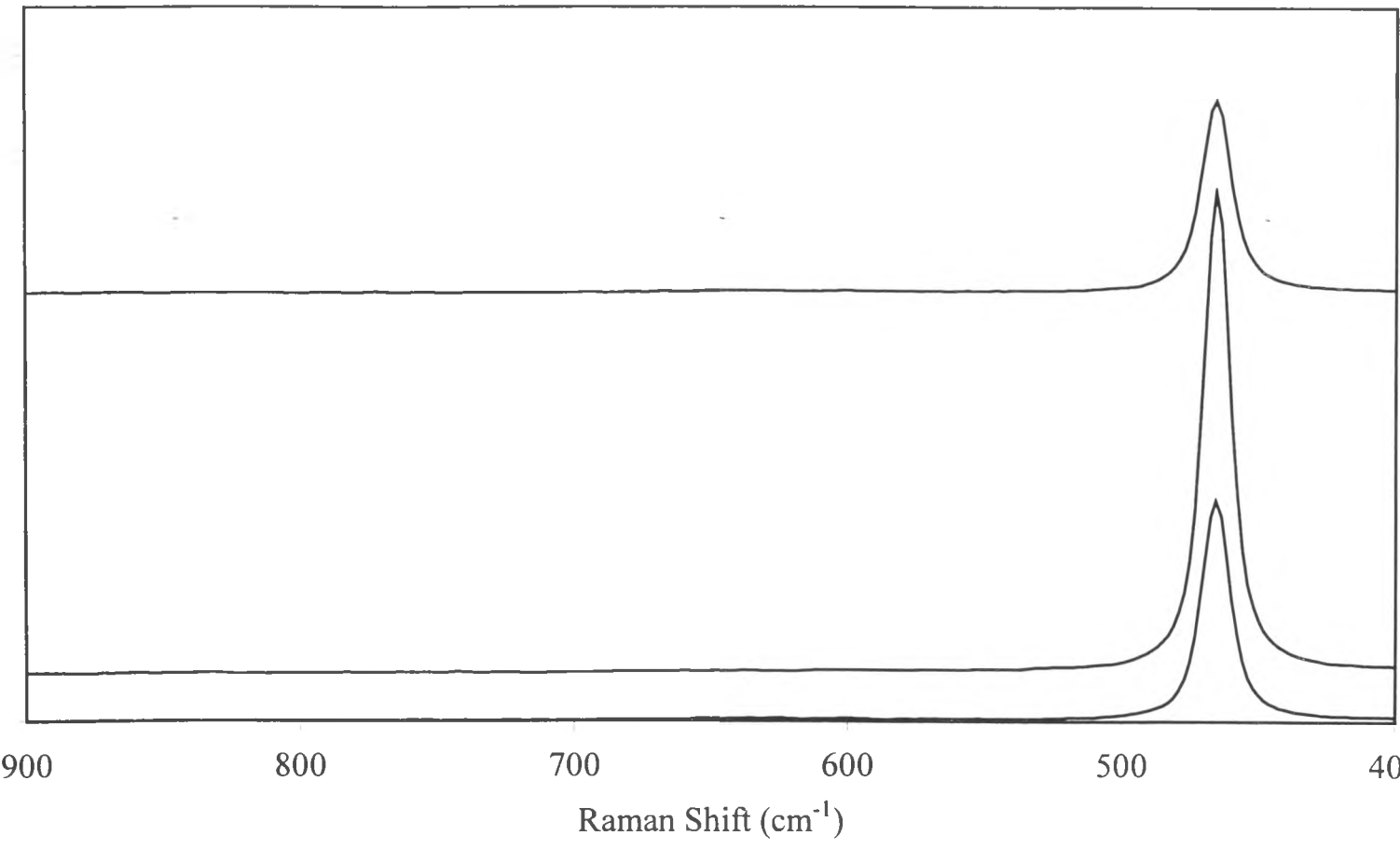

Figure 4.16 FT-Raman Spectra of $Ce_{0.75}Zr_{0.25}O_2$ prepared with different urea concentrations, the reacti
time equal to 120 hours and calcined at 900°C

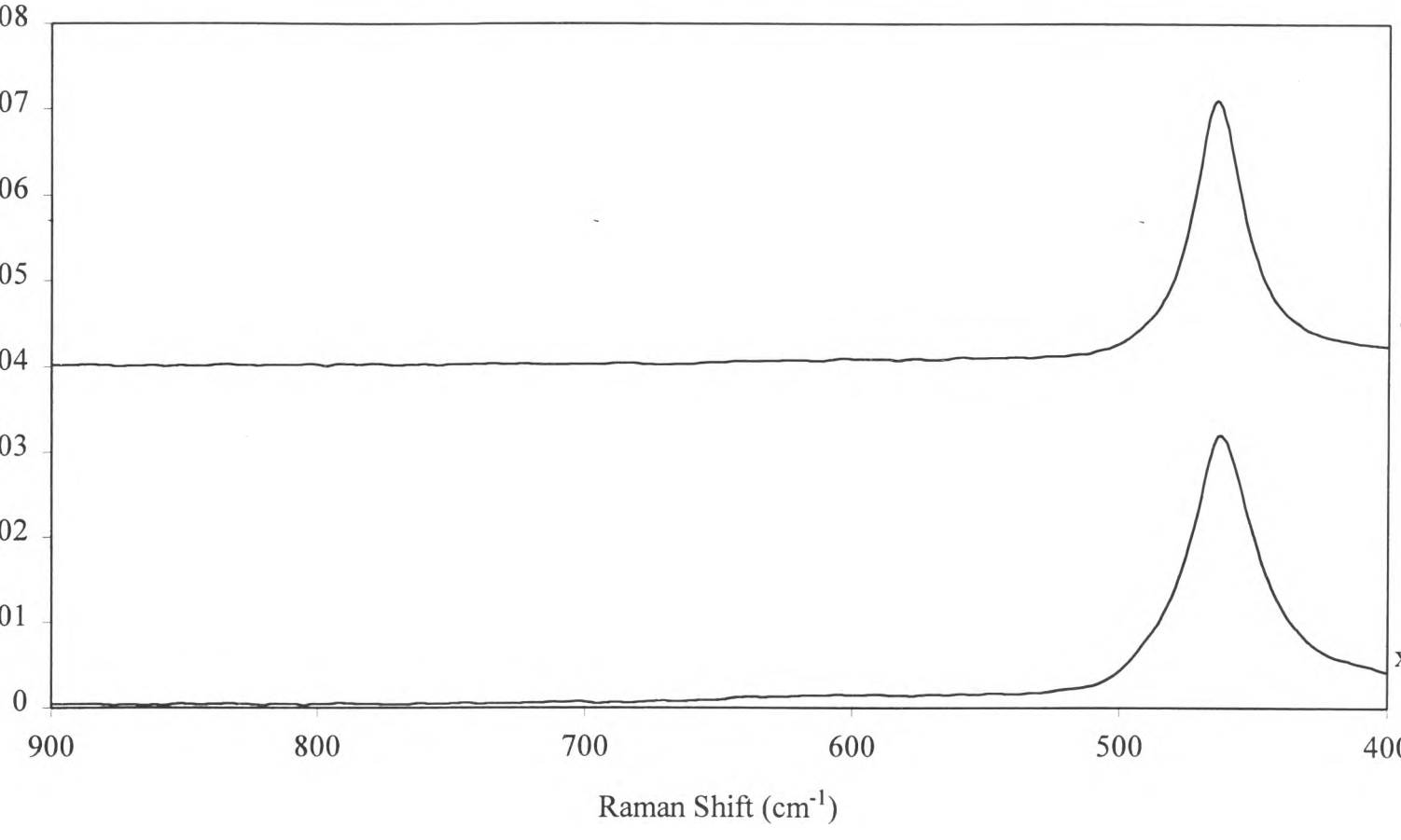

Figure 4.17 FT-Raman Spectra of the xerogel and aerogel of $Ce_{0.75}Zr_{0.25}O_2$ with the reaction time equal to 120 hours and calcined at 500°C

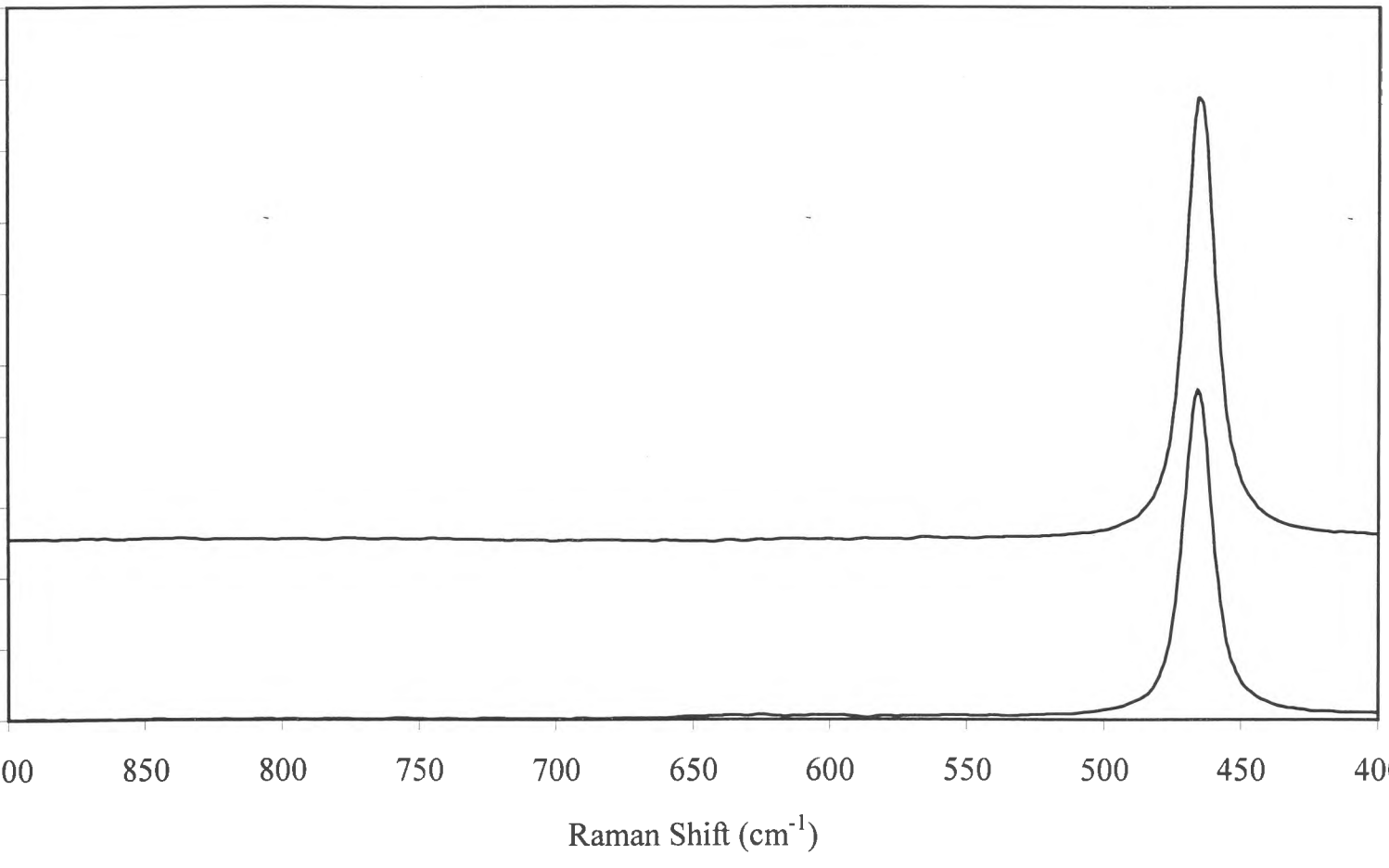

Figure 4.18 FT-Raman Spectra of the xerogel and aerogel of $Ce_{0.75}Zr_{0.25}O_2$ with the reaction time equal t
120 hours and calcined at 900°C

4.4 Scanning Electron Microscope (SEM)

Scanning Electron Microscope (SEM) was used to investigated the morphology of $Ce_{1-x}Zr_xO_2$ (x = 0, 0.25, 0.50, 0.75 and 1.0) catalysts, which are the non-calcined samples, calcined at 500°C samples and calcined at 900°C samples as shown in Figure 4.19 to Figure 4.26.

The shapes of CeO_2 particle are mainly long thin needle shapes, while the shape of pure ZrO_2 are mostly thick sheets. After Zr was incorporated in CeO_2 lattice, the shapes of $Ce_{1-x}Zr_xO_2$ (x = 0.25, 0.50 and 0.75) look like a spherical shape composed of long thin needle shapes. Therefore, $Ce_{0.75}Zr_{0.25}O_2$, $Ce_{0.50}Zr_{0.50}O_2$ and $Ce_{0.25}Zr_{0.75}O_2$ have higher BET surface area than pure CeO_2.

The effects of urea concentration on the morphology of $Ce_{0.75}Zr_{0.25}O_2$, which are non-calcined samples, calcined at 500°C samples and calcined at 900°C samples, were shown in Figure 4.27 to Figure 4.29. The shapes of $Ce_{0.75}Zr_{0.25}O_2$ particles prepared with 0.4M, 1M and 2M are similar, which are long thin needles shape arranged in a spherical shape. This result can confirm BET surface area and XRD results that urea concentration does not affect on the properties of $Ce_{0.75}Zr_{0.25}O_2$.

The particle shapes of the aerogel of $Ce_{0.75}Zr_{0.25}O_2$ and 5%Ni/$Ce_{0.75}Zr_{0.25}O_2$ are similar to $Ce_{0.75}Zr_{0.25}O_2$ as shown in Figure 4.30 and Figure 4.31. For the 5%Ni/$Ce_{0.75}Zr_{0.25}O_2$ sample, no Ni was discovered on the surface of 5%Ni/$Ce_{0.75}Zr_{0.25}O_2$ particles. It is suggesting that Ni is highly dispersed on $Ce_{0.75}Zr_{0.25}O_2$.

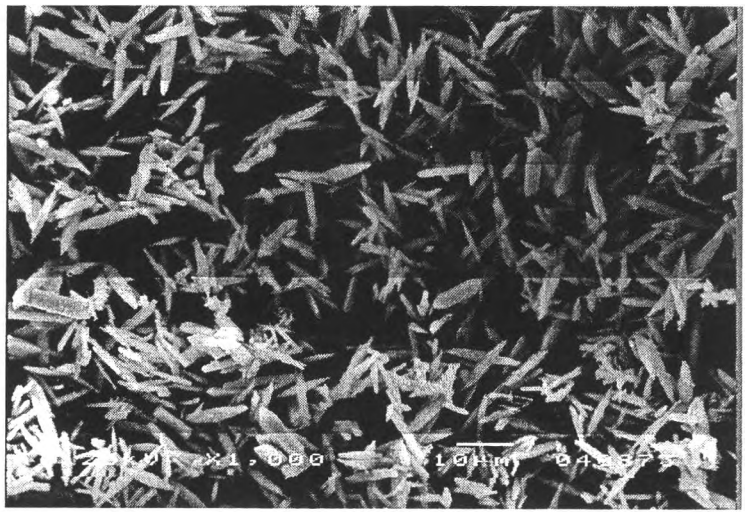

(a)

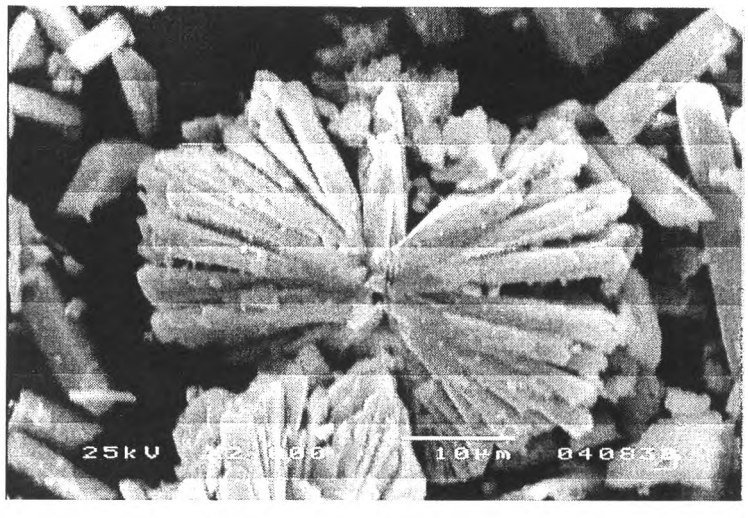

(b)

Figure 4.19 SEM pictures of non-calcined CeO_2 (a) and $Ce_{0.75}Zr_{0.25}O_2$ (b) with the reaction time 120hours.

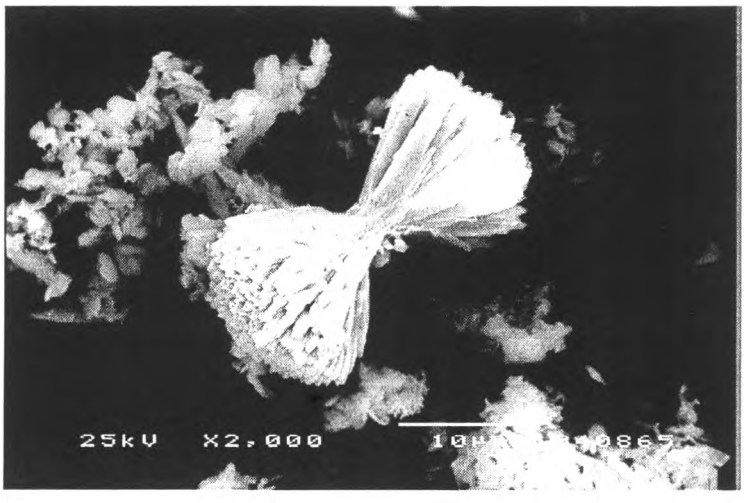

(a)

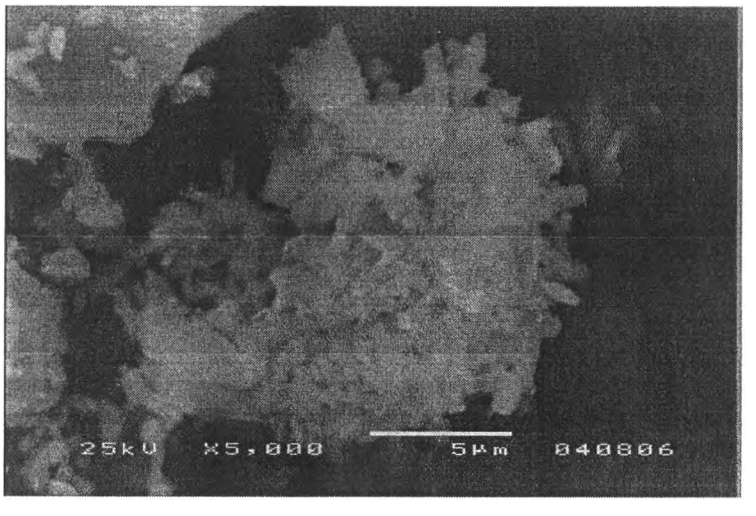

(b)

Figure 4.20 SEM pictures of non-calcined $Ce_{0.50}Zr_{0.50}O_2$ (a) and $Ce_{0.25}Zr_{0.75}O_2$ (b) with the reaction time 120hours.

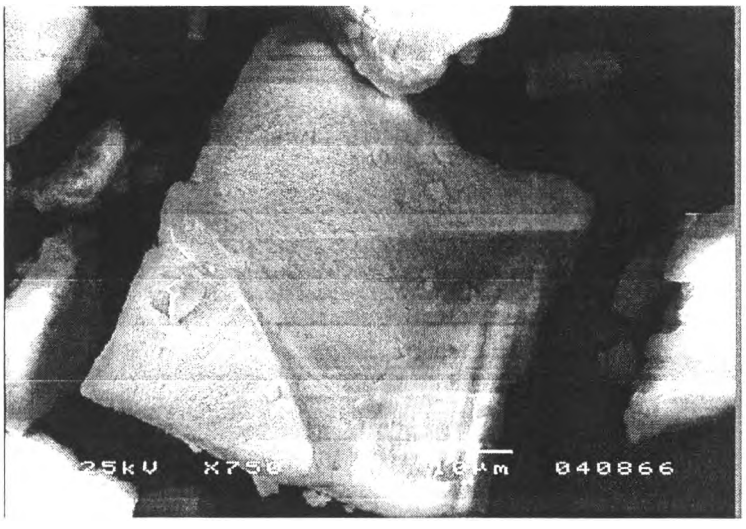

(a)

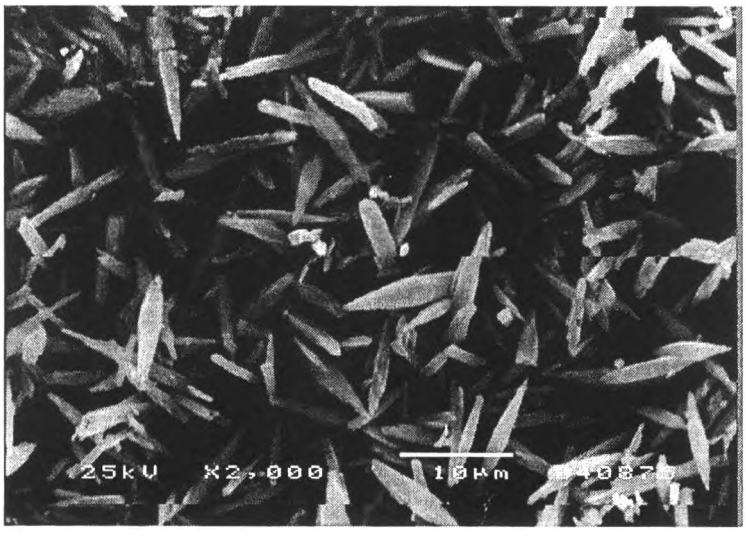

(b)

Figure 4.21 SEM pictures of non-calcined ZrO_2 (a) and CeO_2 calcined at 500°C (b) with the reaction time 120hours.

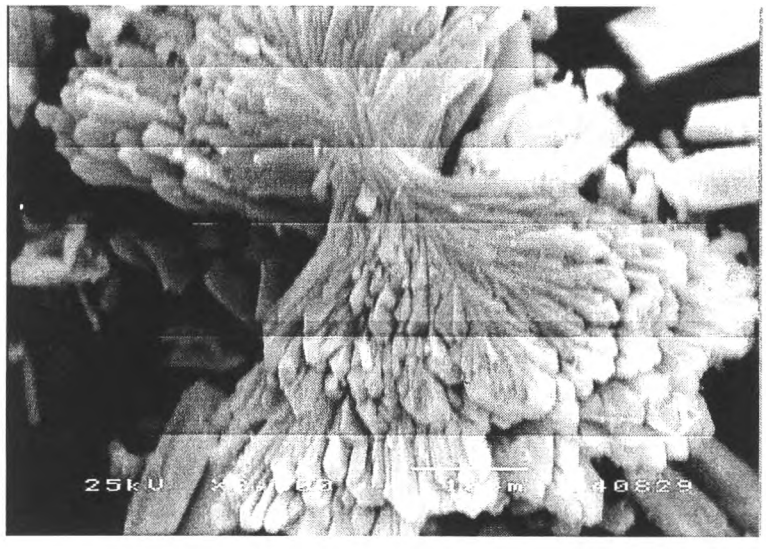

(a)

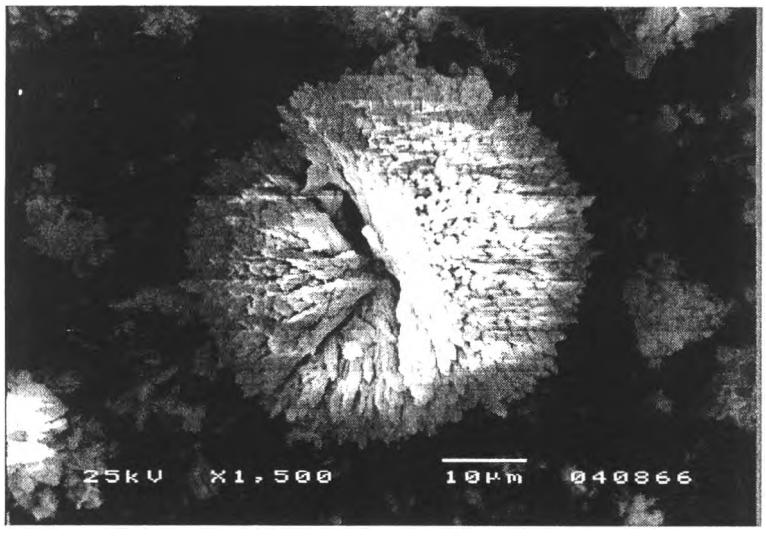

(b)

Figure 4.22 SEM pictures of $Ce_{0.75}Zr_{0.25}O_2$ (a) and $Ce_{0.50}Zr_{0.50}O_2$ (b) with the reaction time 120hours and calcined at 500°C.

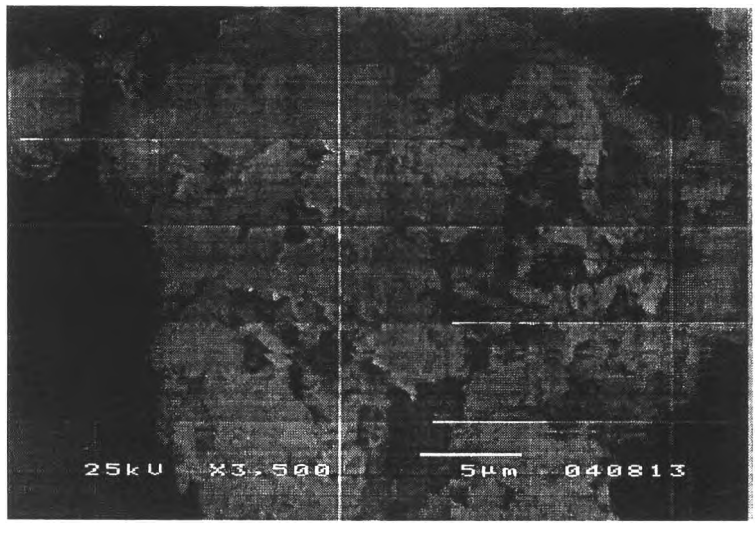

(a)

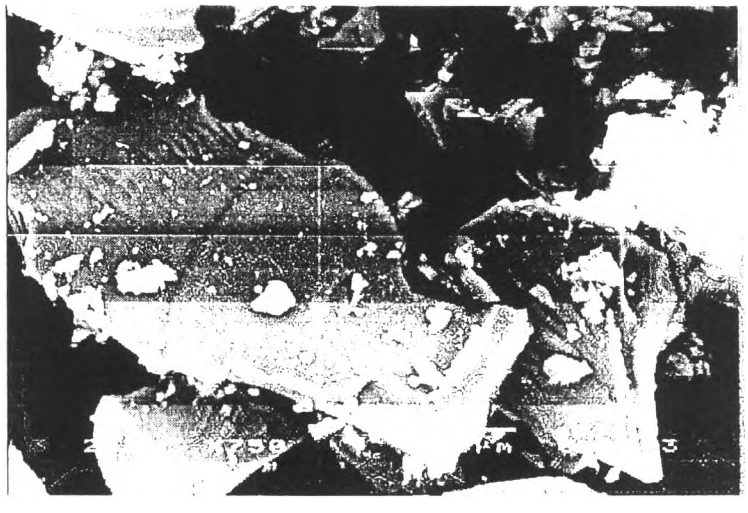

(b)

Figure 4.23 SEM pictures of $Ce_{0.25}Zr_{0.75}O_2$ calcined at 500°C (a) and ZrO_2 calcined at 900°C (b) with the reaction time 120hours and calcined at 500°C.

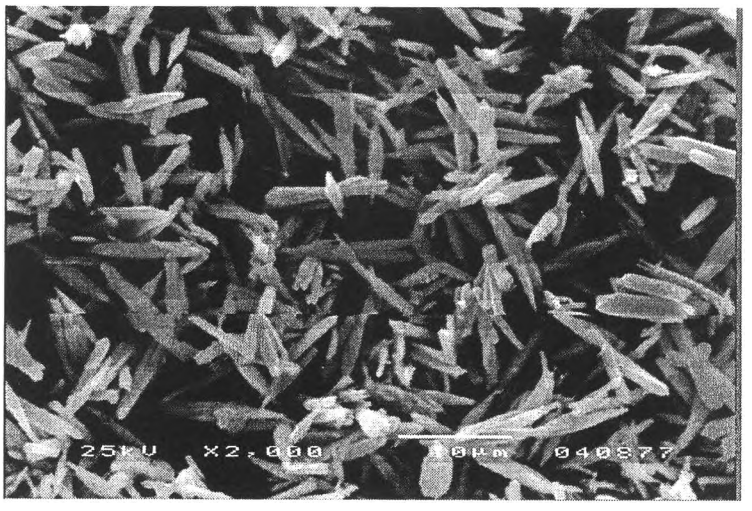

(a)

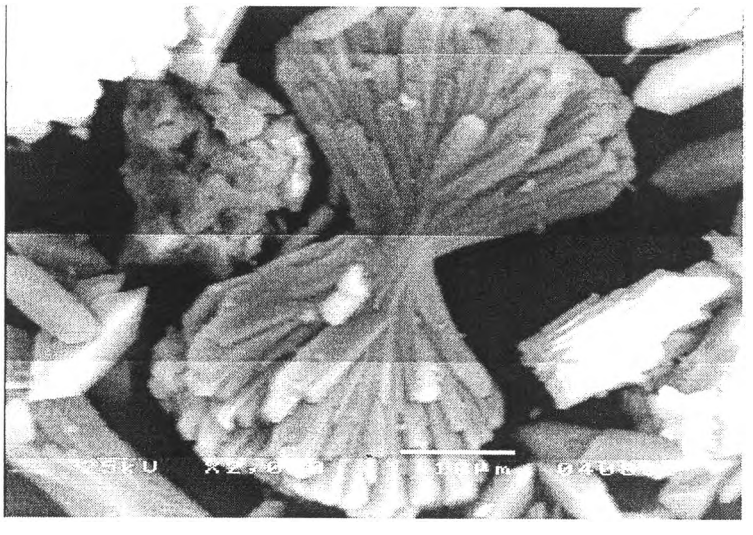

(b)

Figure 4.24 SEM pictures of CeO_2 (a) and $Ce_{0.75}Zr_{0.25}O_2$ (b) with the reaction time 120hours and calcined at 900°C.

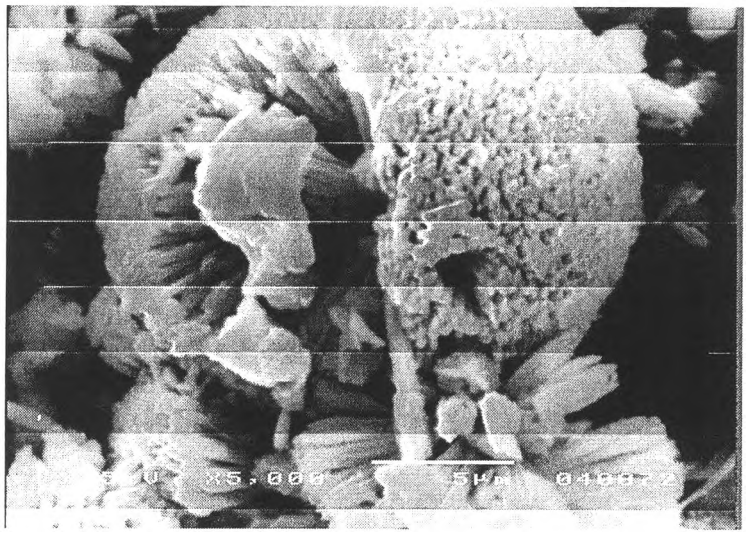

(a)

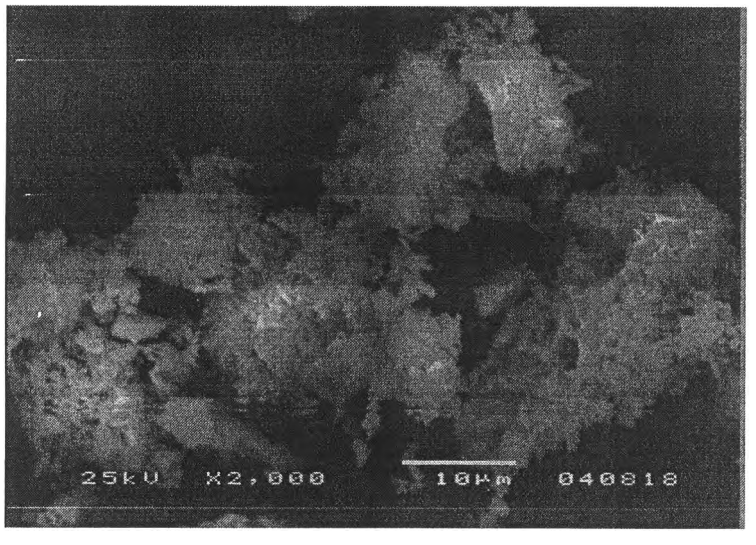

(b)

Figure 4.25 SEM pictures of $Ce_{0.50}Zr_{0.50}O_2$ (a) and $Ce_{0.25}Zr_{0.75}O_2$ (b) with the reaction time 120hours calcined at 900°C.

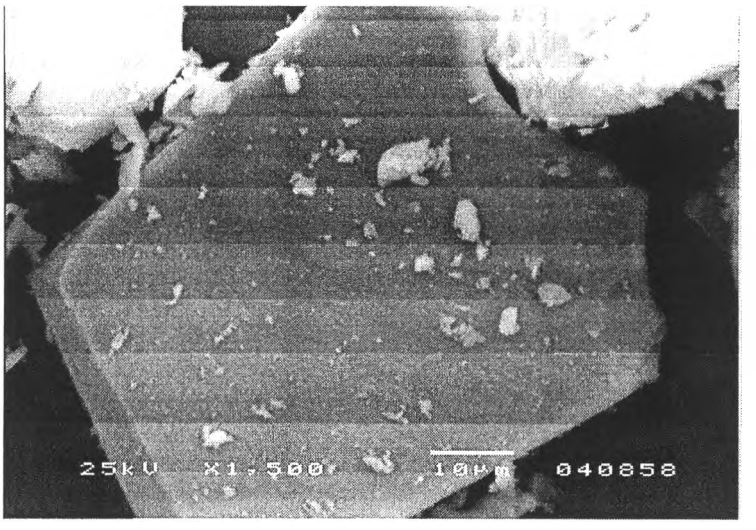

Figure 4.26 SEM pictures of ZrO_2 with the reaction time 120hours calcined at 900°C.

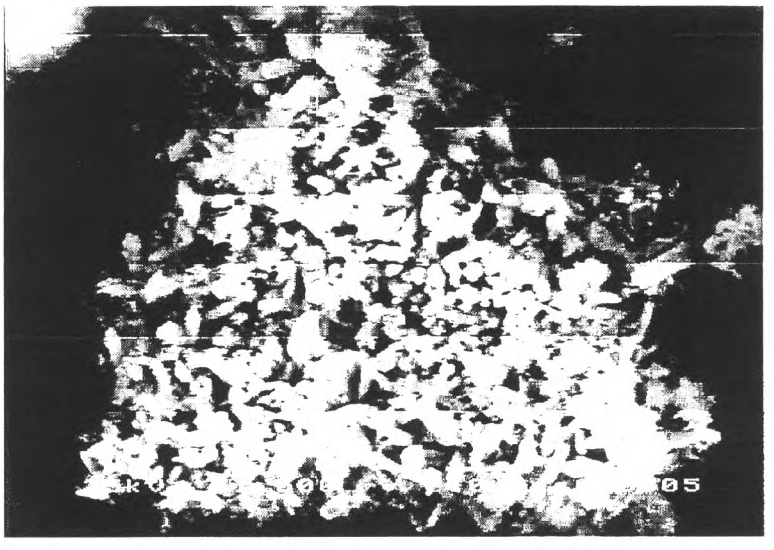

(a)

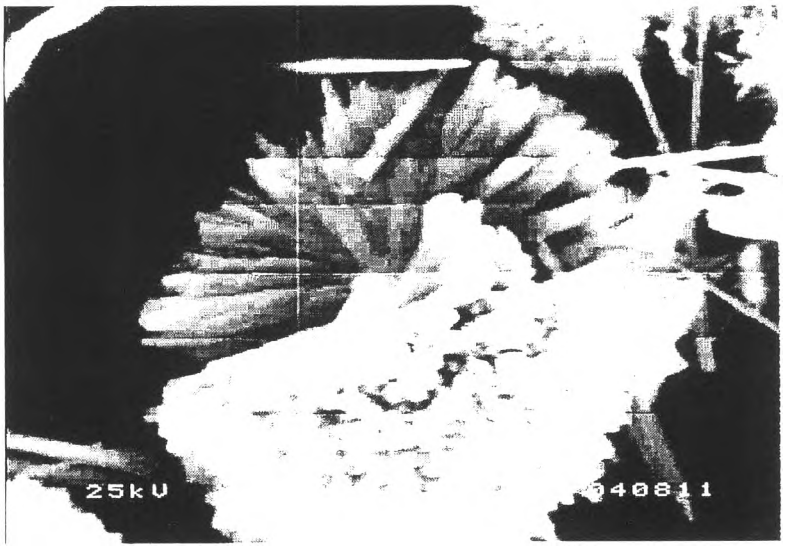

(b)

Figure 4.27 SEM pictures of non-calcined $Ce_{0.75}Zr_{0.25}O_2$ prepared with 1M urea (a) and 2M urea (b), reaction time 120hours.

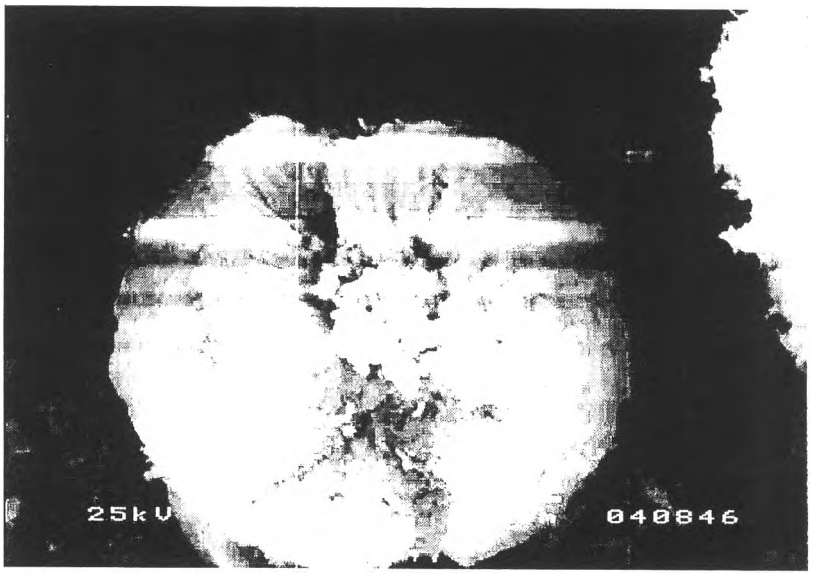

(a)

(b)

Figure 4.28 SEM pictures of $Ce_{0.75}Zr_{0.25}O_2$ prepared with 1M urea (a) and 2M urea (b), reaction time 120hours calcined at 500°C.

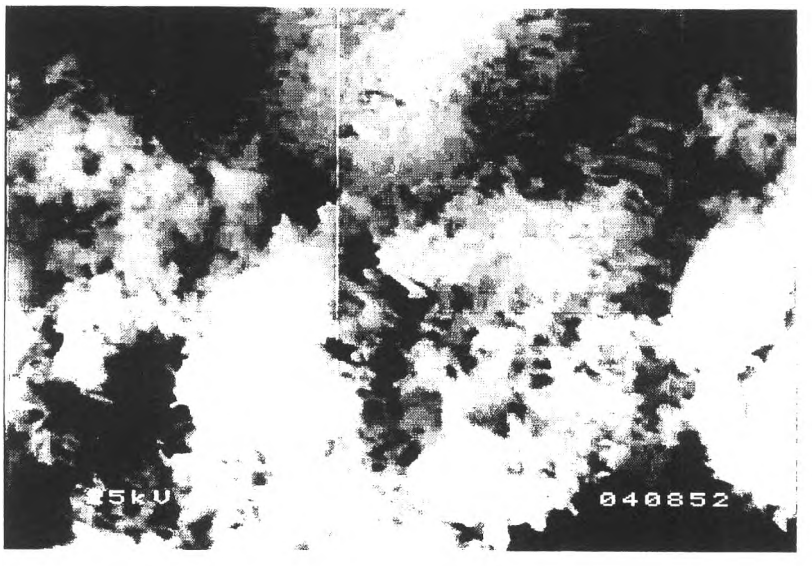

(a)

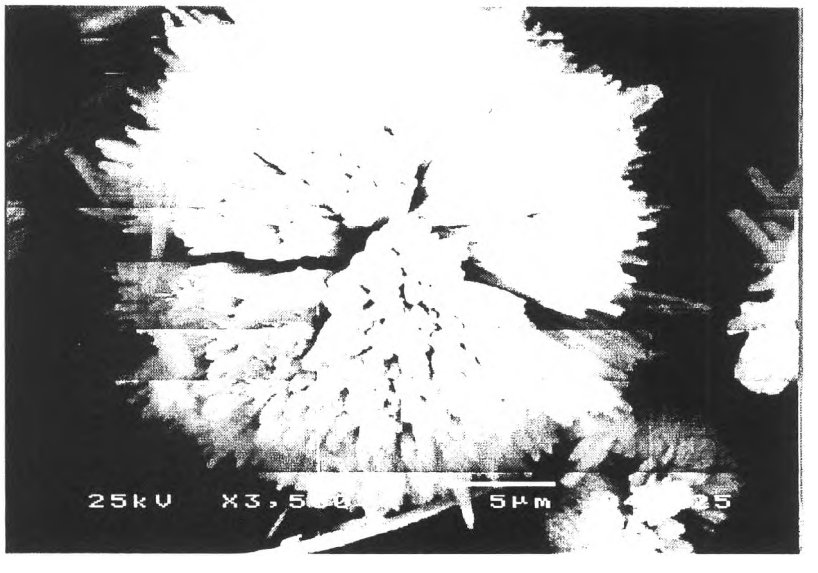

(b)

Figure 4.29 SEM pictures of $Ce_{0.75}Zr_{0.25}O_2$ prepared with 1M urea (a) and 2M urea (b), reaction time 120hours calcined at 900°C.

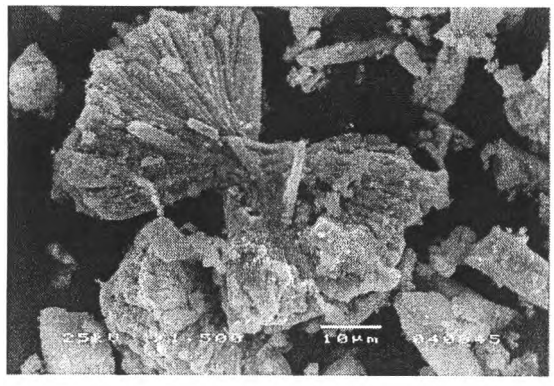

(a)

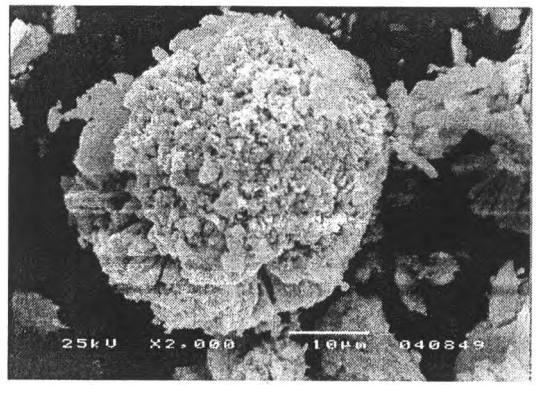

(b)

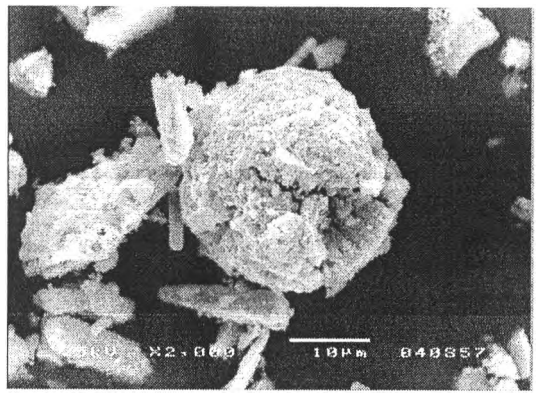

(c)

Figure 4.30 SEM pictures of the aerogel of $Ce_{0.75}Zr_{0.25}O_2$ prepared with 0.4M urea, reaction time 120hours non-calcined (a), calcined at 500°C (b) and calcined at 900°C (c).

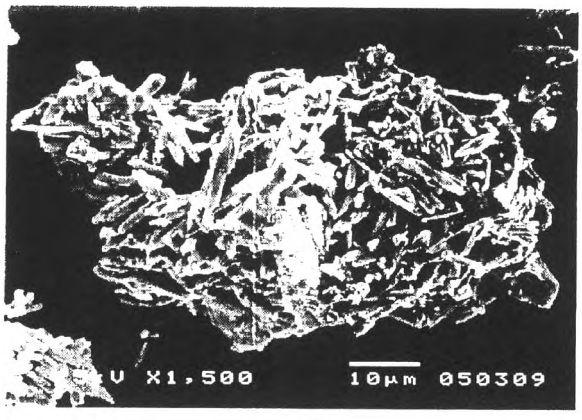

(a)

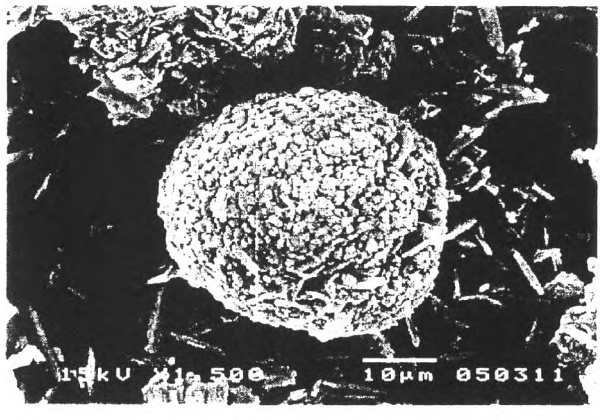

(b)

(c)

Figure 4.31 SEM pictures of 5%Ni/$Ce_{0.75}Zr_{0.25}O_2$ prepared with 0.4M urea, reaction time 120hours and non-calcined (a), calcined at 500°C (b), and calcined at 900°C (c).

4.5 Catalyst Testing

4.5.1 Iso-octane Oxidation over $Ce_{1-x}Zr_xO_2$

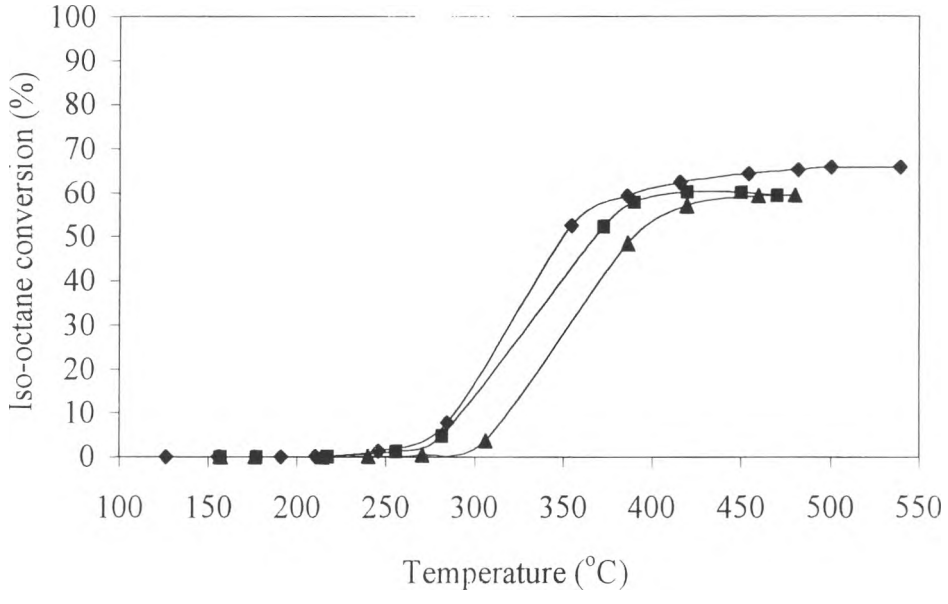

Figure 4.32 Light off temperature of iso-octane oxidation at O_2/C ratio = 1/1 over $Ce_{1-x}Zr_xO_2$ with reaction time 120 hours and calcined at 500°C: (◆) $Ce_{0.75}Zr_{0.25}O_2$, (■) $Ce_{0.50}Zr_{0.50}O_2$ and (▲) $Ce_{0.25}Zr_{0.75}O_2$.

$Ce_{1-x}Zr_xO_2$ (x = 0.25, 0.50 and 0.75) with reaction time 120 hours and calcined at 500°C were the catalytic activity for iso-octane oxidation at O_2/C of 1/1. All catalysts have similar light off pattern. The shape of light off temperature can be divided into 3 regions. First, the iso-octane conversion slightly increases at low temperature. Then, the conversion rises sharply and increases slowly to the final conversion. The final conversion did not reach 100% iso-octane conversion because the oxygen is consumed up.

Light off temperature of ca. 340, 360 and 390 were observed for $Ce_{0.75}Zr_{0.25}O_2$, $Ce_{0.50}Zr_{0.50}O_2$ and $Ce_{0.25}Zr_{0.75}O_2$, respectively. It is found that $Ce_{0.75}Zr_{0.25}O_2$ has the lowest light off temperature compared to the other two catalysts. Thus, $Ce_{0.75}Zr_{0.25}O_2$ has the highest catalytic activity for iso-octane oxidation.

This occurrence can be explained by the XRD results (Figure 4.2). Only XRD pattern of $Ce_{0.75}Zr_{0.25}O_2$ is similar to the cubic fluorite structured of CeO_2, while the characteristic of tetragonality was observed in the XRD pattern of $Ce_{0.50}Zr_{0.50}O_2$ and $Ce_{0.25}Zr_{0.75}O_2$. It can be summarized that the solid solution of Ce and Zr is mainly found in $Ce_{0.75}Zr_{0.25}O_2$, and small amount of solid solution was observed in $Ce_{0.50}Zr_{0.50}O_2$ and $Ce_{0.25}Zr_{0.75}O_2$. As reported by Fornasiero *et al.* (1996), $Ce_{1-x}Zr_xO_2$ with high solid solution can be reduced easily even at low temperature. Thus, $Ce_{0.75}Zr_{0.25}O_2$ with the lowest light off temperature has the best activity for iso-octane oxidation.

4.5.2 The Light off Temperature over $Ce_{0.75}Zr_{0.25}O_2$ Calcined at 500°C and 900°C

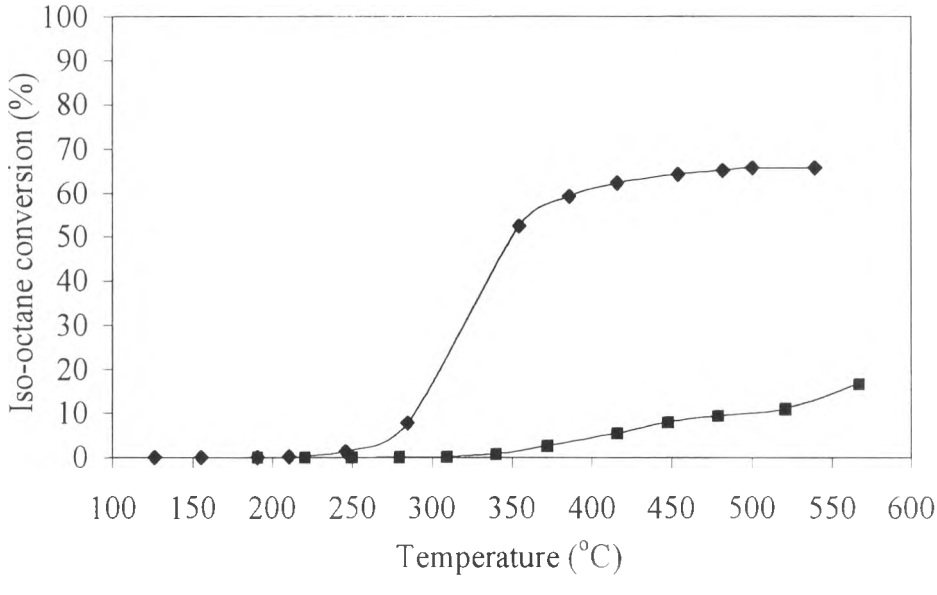

Figure 4.33 Light off temperature of iso-octane oxidation at O_2/C ratio = 1/1 over $Ce_{0.75}Zr_{0.25}O_2$ calcined at (◆) 500°C and (■) 900°C.

The light off temperature of iso-octane oxidation at O_2/C ratio equal to 1/1 over $Ce_{0.75}Zr_{0.25}O_2$ with reaction time 120 hours and calcined at 500°C and 900°C is presented in Figure 4.37. The light off temperature of 440°C was observed for $Ce_{0.75}Zr_{0.25}O_2$ calcined at 500°C, while the light off temperature for the sample calcined at 900°C can not observe in this range of temperature.

$Ce_{0.75}Zr_{0.25}O_2$ calcined at 500°C has better activity for iso-octane oxidation than that calcined at 900°C. Therefore, $Ce_{0.75}Zr_{0.25}O_2$ was selected for further study.

4.5.3 The Light off Temperature over Xerogel and Aerogel of $Ce_{0.75}Zr_{0.25}O_2$

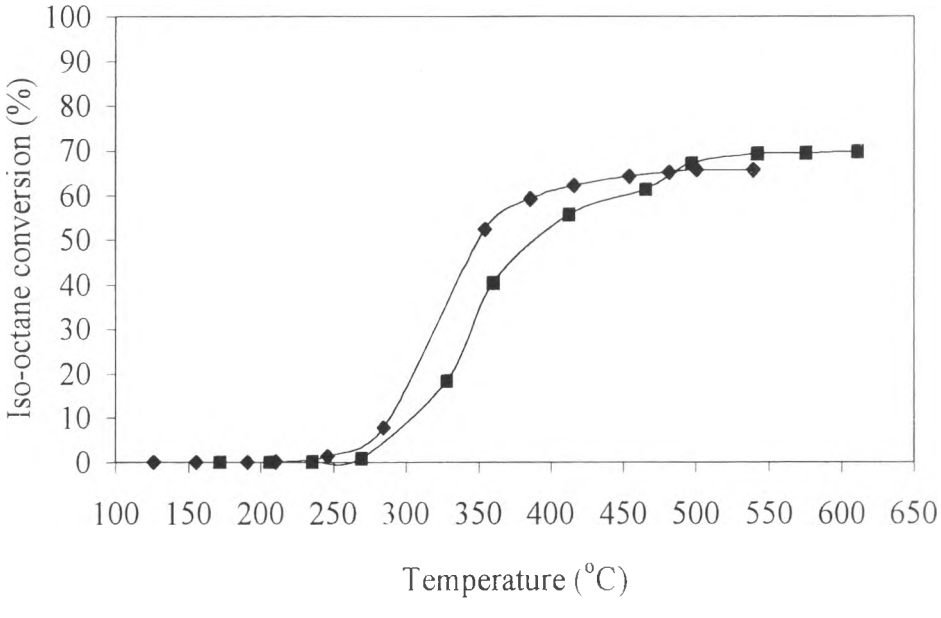

Figure 4.34 Light off temperature of iso-octane oxidation at O_2/C ratio = 1/1 over (◆) xerogel of $Ce_{0.75}Zr_{0.25}O_2$ and (■) aerogel of $Ce_{0.75}Zr_{0.25}O_2$ with reaction time 120 hours and calcined at 500°C.

Figure 4.33 shows the light off temperature of C_8H_{18} oxidation over xerogel of $Ce_{0.75}Zr_{0.25}O_2$ and aerogel of $Ce_{0.75}Zr_{0.25}O_2$ with reaction time 120 hours and calcined at 500°C. The light of temperature of ca. 340 and 390°C were observed for xerogel of $Ce_{0.75}Zr_{0.25}O_2$ and aerogel of $Ce_{0.75}Zr_{0.25}O_2$, respectively. The $Ce_{0.75}Zr_{0.25}O_2$ has the lower light off temperature than the aerogel of $Ce_{0.75}Zr_{0.25}O_2$. It is suggesting that xerogel of $Ce_{0.75}Zr_{0.25}O_2$ has better catalytic activity than aerogel of $Ce_{0.75}Zr_{0.25}O_2$ Therefore, 5% Ni was loaded on the xerogel of $Ce_{0.75}Zr_{0.25}O_2$.

4.5.5 The Light off Temperature over $Ce_{0.75}Zr_{0.25}O_2$ and 5%Ni/ $Ce_{0.75}Zr_{0.25}O_2$

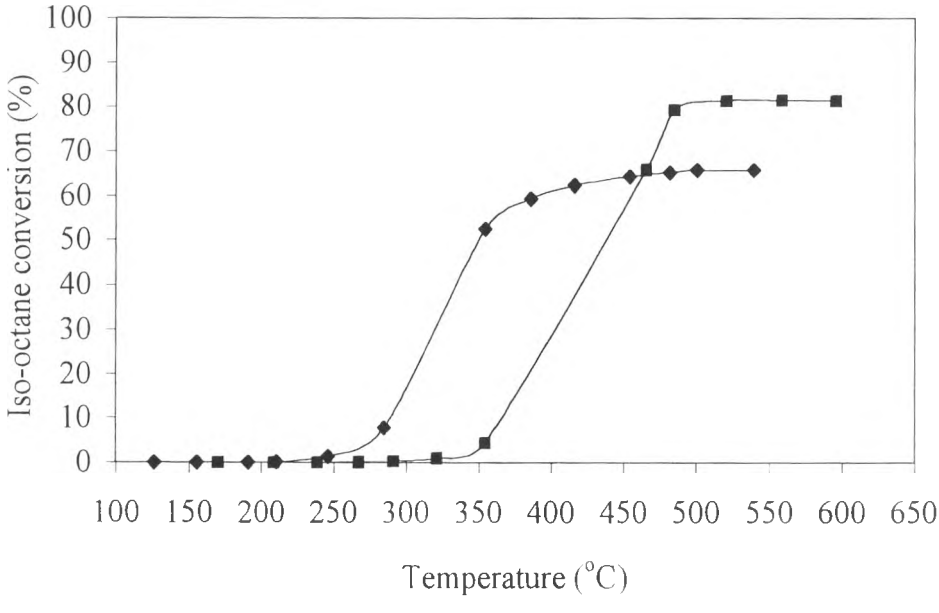

Figure 4.35 Light off temperature of iso-octane oxidation at O_2/C ratio = 1/1 over (◆) $Ce_{0.75}Zr_{0.25}O_2$ and (■) 5%Ni/$Ce_{0.75}Zr_{0.25}O_2$ with reaction time 120 hours and calcined at 500°C.

After $Ce_{0.75}Zr_{0.25}O_2$ prepared with 0.4M urea at the reaction time 120 hours and calcined at 500°C was proven to be the most active catalyst for iso-octane oxidation, 5%Ni was loaded on $Ce_{0.75}Zr_{0.25}O_2$. Figure 4.35 shows the light off temperature of iso-octane oxidation at O_2/C ratio =

1/1 over $Ce_{0.75}Zr_{0.25}O_2$ and 5%Ni/$Ce_{0.75}Zr_{0.25}O_2$ with reaction time 120 hours and calcined at 500°C. Surprisingly, 5%Ni/$Ce_{0.75}Zr_{0.25}O_2$ has higher light off temperature than that of $Ce_{0.75}Zr_{0.25}O_2$. In the other word, 5%Ni/$Ce_{0.75}Zr_{0.25}O_2$ has lower catalytic activity than $Ce_{0.75}Zr_{0.25}O_2$. However, the higher iso-octane conversion was obtained from 5%Ni/$Ce_{0.75}Zr_{0.25}O_2$ at high temperature.

The increase in iso-octane oxidation at high temperature by using 5%Ni/$Ce_{0.75}Zr_{0.25}O_2$ can be explained by the product selectivity of each catalyst. Figure 4.36 and 4.37 show the product selectivity obtained from iso-octane oxidation over $Ce_{0.75}Zr_{0.25}O_2$ and 5%Ni/$Ce_{0.75}Zr_{0.25}O_2$, respectively. The main product obtained from iso-octane oxidation over $Ce_{0.75}Zr_{0.25}O_2$ and is CO_2, while little yield of CO was observed in the range of ca.280-350°C as shown in Figure 4.36. The presence of CO product cause a slightly drop in CO_2 product selectivity in the range of ca.280-350°C (Figure 4.36a)) For 5%Ni/$Ce_{0.75}Zr_{0.25}O_2$, CO_2 is the main product in the first range of temperature. Then, CO and H_2 were observed when the temperature is higher than 450°C (Figure 4.37). It can be concluded that 5%Ni/$Ce_{0.75}Zr_{0.25}O_2$ can enhances the partial oxidation reaction (2.11) of iso-octane, resulting in higher conversion of iso-octane at high temperature. Moreover, high selectivity of H_2 was achieved from the oxidation of iso-octane over 5%Ni/$Ce_{0.75}Zr_{0.25}O_2$ catalyst. While no H_2 was observed from iso-octane oxidation over $Ce_{0.75}Zr_{0.25}O_2$.

In case of 5%Ni/$Ce_{0.75}Zr_{0.25}O_2$, the observed H_2/CO ratio (ca 3.5-5.0) is higher than 2, which is stoichiometric ratio of H_2/CO product ratio in partial oxidation reaction. It is suggesting that H_2 can not be produced from partial oxidation only. Otsuka *et al.* (1999) reported that the H_2/CO ratio being higher than 2 indicated the deposition of carbonaceous species. C_8H_{18} is decomposed to carbonaceous species at high temperature. By the presence of Ce^{3+} sites in the catalyst, carbonaceous species, which is a reaction intermediate, will be oxidized to H_2 and CO. Therefore, H_2 can be produced

from partial oxidation reaction and the decomposition of carbonaceous species, resulting in high H_2/CO product ratio (> 2).

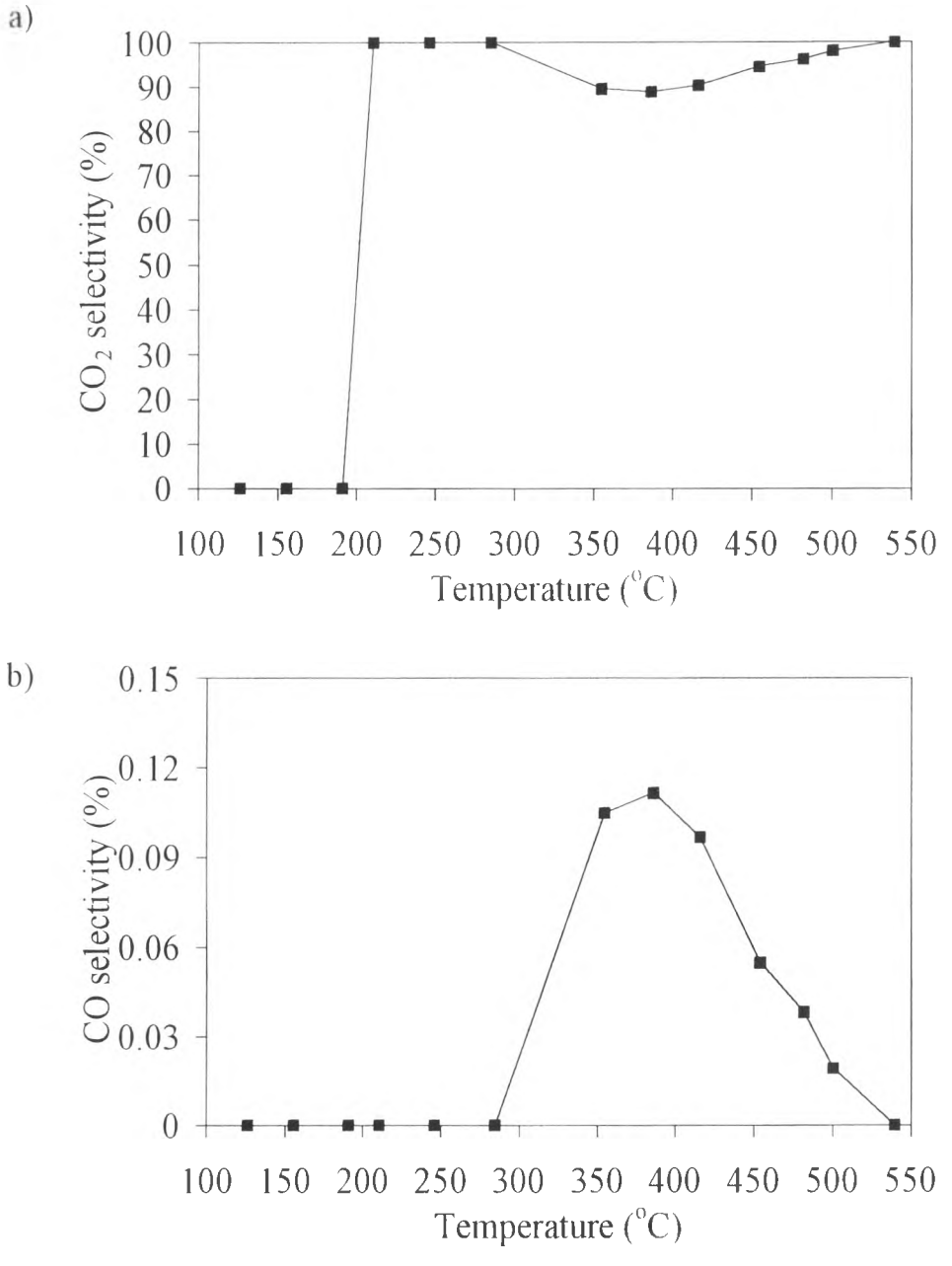

Figure 4.36 Selectivity of CO_2 and Selectivity of CO product from iso-octane oxidation at O_2/C =1/1 over $Ce_{0.75}Zr_{0.25}O_2$ with reaction time 120 hours calcined at 500°C; a) CO_2 selectivity and b) CO selectivity

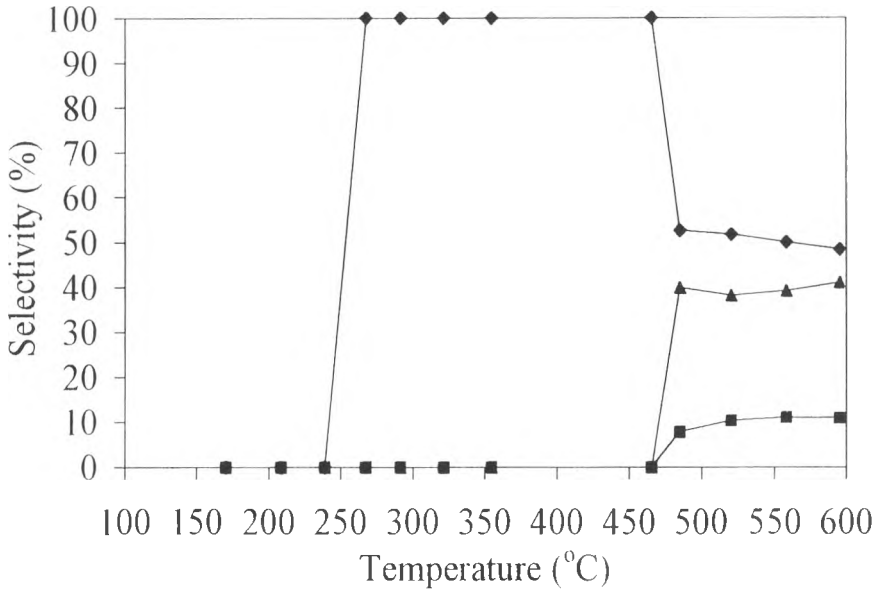

Figure 4.37 Selectivity of CO_2, CO and H_2 product from iso-octane oxidation at O_2/C ratio = 1/1 over 5%Ni/$Ce_{0.75}Zr_{0.25}O_2$ with reaction time 120 hours calcined at 500°C; (◆) CO_2, (■) CO and (▲) H_2.

4.5.6 The Effect of O_2/C Ratio on Light off Temperature over 5%Ni/$Ce_{0.75}Zr_{0.25}O_2$

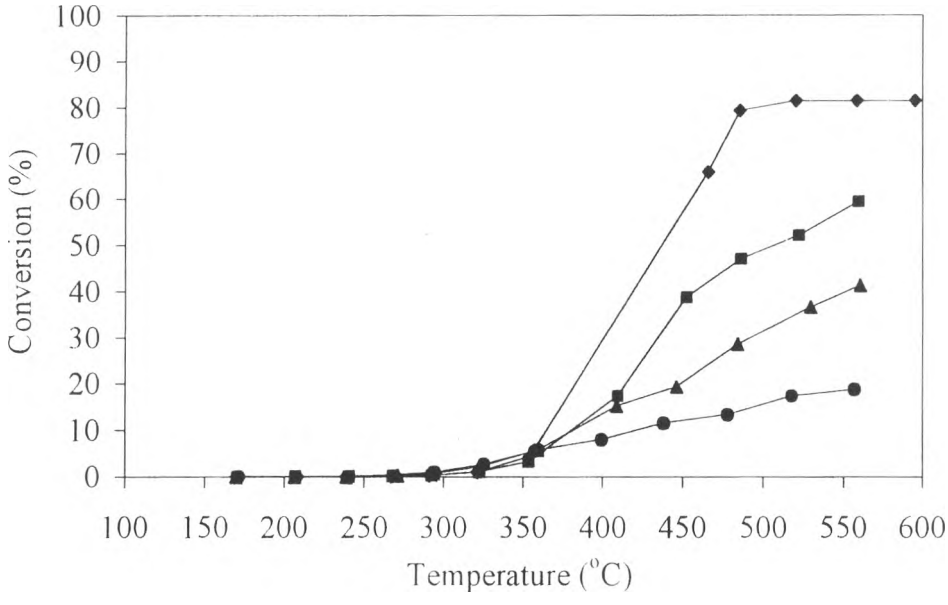

Figure 4.38 The effect of O_2/C on light off temperature of iso-octane oxidation over 5%Ni/$Ce_{0.75}Zr_{0.25}O_2$; O_2/C ratios: (●) 0.125/1, (▲) 0.25/1, (■) 0.50/1 and (◆) 1/1.

In autothermal system, heat generated from partial oxidation reaction will be supplied to steam-reforming reaction. Therefore, O_2/C ratio was varied from 0.125, 0.25, 0.50 and 1, which was not exceeded the O_2/C stoichiometric ratio for iso-octane partial oxidation (O_2/C=1.2).

Figure 4.38 shows the effect of O_2/C on light off temperature of iso-octane oxidation over 5%Ni/$Ce_{0.75}Zr_{0.25}O_2$. The similar light off patterns was observed for each O_2/C ratio. The light off temperature of 440°C and 520°C were observed for O_2/C ratio of 0.5/1 and 1/1. The light off temperature for O_2/C ratio of 0.125/1 and 0.25/1 can not observed in this temperature range. It is observed that the iso-octane conversion increases with increasing O_2/C ratio. The highest catalytic activity of 5%Ni/$Ce_{0.75}Zr_{0.25}O_2$ for iso-octane oxidation was obtained at O_2/C ratio of 1/1.

4.6 The Effect of Steam/Carbon Ratios

Figure 4.39 shows the influence of steam/carbon ratios on the H_2/CO product ratio in autothermal system of iso-octane over 5%Ni/$Ce_{0.75}Zr_{0.25}O_2$ catalyst. The experiment is done at constant O_2/C ratio = 1/1 on account of 5%Ni/$Ce_{0.75}Zr_{0.25}O_2$ exhibited the highest catalytic activity for iso-octane oxidation at O_2/C of 1/1.

H_2 can be produced at the temperature above 450°C. The observed H_2/CO ratio (>8.375) indicated that water-gas shift reaction occurred simultaneously with steam reforming reaction. Moreover, H_2/CO product ratio strongly depends on the concentration of steam at low temperature (450-500°C). While H_2/CO ratio was slightly changed with the increase in H_2O/C ratio at temperature above 550°C. However, H_2/CO ratio decreases with increasing temperature. This result is correspondent with the fact that water-gas shift reaction is not thermodynamically favored at high temperature (Choudhary *et al.*, 1998). Figure 4.40 can confirm this explanation.

Figure 4.40 shows the effect of H_2O/C ratio on CO selectivity. CO selectivity increases with increasing temperature. However, CO selectivity decreases when the steam concentration increases. It is suggesting that the partial oxidation might be inhibited by the addition of steam. In addition, the increase in steam/carbon ratio enhances the water-gas shift reaction rate, but decreases the concentration of CO. Since CO is the reactant in the water-gas shift reaction. The increase in CO selectivity with a rise in temperature was by the decrease of the rate of water-gas shift, which is not thermodynamically favored at high temperature.

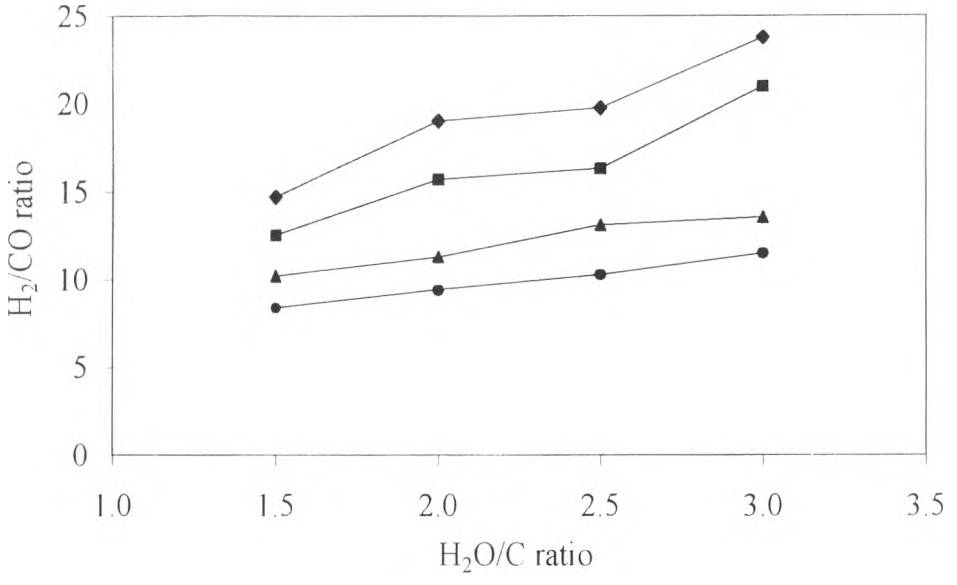

Figure 4.39 The effect of H_2O/C ratios on H_2/CO product ratio at (◆) 450°C, (■) 500°C, (▲) 550°C and (●) 600°C of 5%Ni/$Ce_{0.75}Zr_{0.25}O_2$ at O_2/C =1/1.

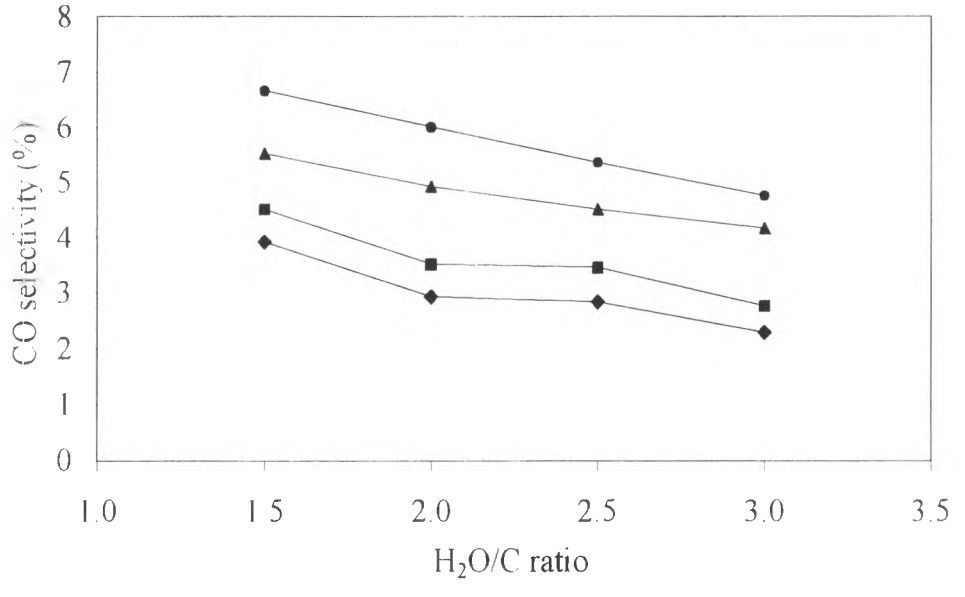

Figure 4.40 The effect of H_2O/C ratios on CO selectivity at (◆) 450°C, (■) 500°C, (▲) 550°C and (●) 600°C of 5%Ni/$Ce_{0.75}Zr_{0.25}O_2$ at O_2/C = 1/1.

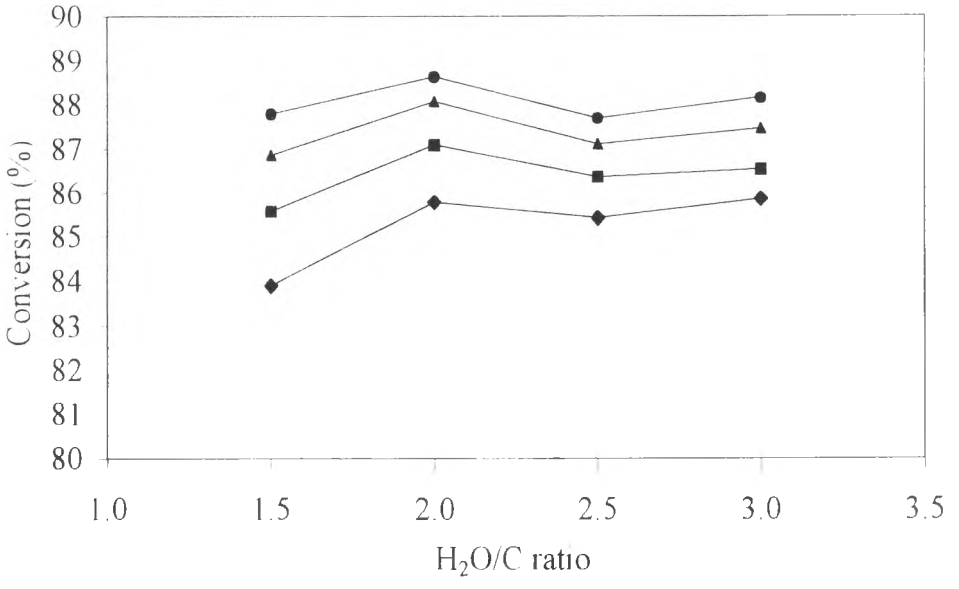

Figure 4.41 The effect of H_2O/C on iso-octane conversion at (◆) 450°C, (■) 500°C, (▲) 550°C and (●) 600°C over 5%Ni/$Ce_{0.75}Zr_{0.25}O_2$ at O_2/C ratio 1/1.

As shown in Figure 4.41, the iso-octane conversion is slightly effected by H_2O/C ratio. The iso-octane conversion increases with increasing temperature because of the increasing of the rate of steam reforming and partial oxidation. The iso-octane conversions slightly increase when the H_2O/C ratio increases from 1.5 to 2.0. Then, the conversion is slightly dropped at H_2O/C ratio above 2.0. This may be due to the addition of steam inhibited the oxidation reaction resulting in the decrease of conversion. Furthermore, the iso-octane conversion with the addition of steam increases a little bit from that obtained from the oxidation of iso-octane over 5%Ni/$Ce_{0.75}Zr_{0.25}O_2$ as presented in Figure 4.34. It can be concluded that the oxidation is the main reaction in autothermal system.

4.7 The Effect of Oxygen/Carbon Ratios

The effect of O_2/C ratio on the H_2/CO in autothermal system of iso-octane over $5\%Ni/Ce_{0.75}Zr_{0.25}O_2$ was presented in Figure 4.42. The experiment was carried at H_2O/C at 2/1 because the highest iso-octane conversion was obtained at this H_2O/C.

The H_2/CO ratio was hardly effected by the O_2/C ratio. H_2/CO ratio gradually increases with increasing O_2/C ratios. It is suggesting that ceria (CeO_2) acts as an oxygen storage that can store and release oxygen at lean and rich condition. The increase in H_2/CO ratio corresponds to the decrease in CO selectivity (Figure 4.43). The observed H_2/CO ratio (~6.0-12.0) shows that steam reforming, water gas shift reaction occurred simultaneously. The decrease in H_2/CO ratio with a rise in temperature was caused by the decrease in the rate of water-gas shift reaction at high temperature.

As shown in Figure 4.42, the increasing of oxygen/carbon ratio dropped CO selectivity. It can be indicated that the increase in O_2/C ratio inhibited the rate of partial oxidation reaction, resulting in the decrease of CO selectivity. Temperature also influences on the CO selectivity. The increase in temperature increases CO selectivity. Since CO is the reactant in water-gas shift reaction. The increase in temperature suppresses the rate of water-gas shift that enhances the increase in CO concentration.

The influence of O_2/C ratio on the iso-octane conversion is performed in Figure 4.43. The iso-octane conversion was strongly effected by the O_2/C ratio. It can be concluded that the main reaction in the autothermal system with $5\%Ni/Ce_{0.75}Zr_{0.25}O_2$ is iso-octane oxidation. Moreover, the increase in temperature increases the conversion of iso-octane. It is showed that the rate of iso-octane oxidation and steam reforming was enhanced at high temperature.

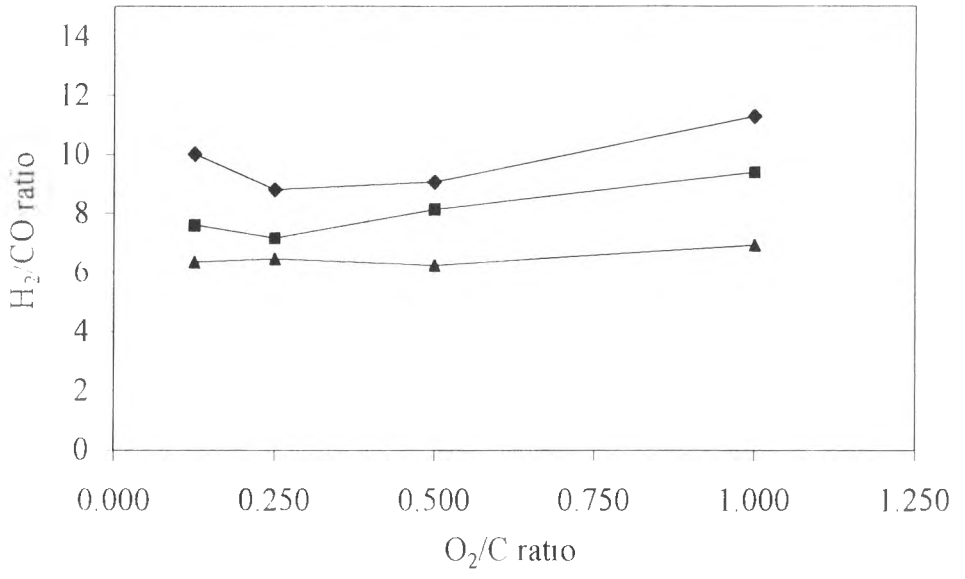

Figure 4.42 The effect of O_2/C ratios on H_2/CO production ratio at (◆) 550°C, (■) 600°C and (▲) 650°C over 5%Ni/$Ce_{0.75}Zr_{0.25}O_2$ at H_2O/C = 2/1

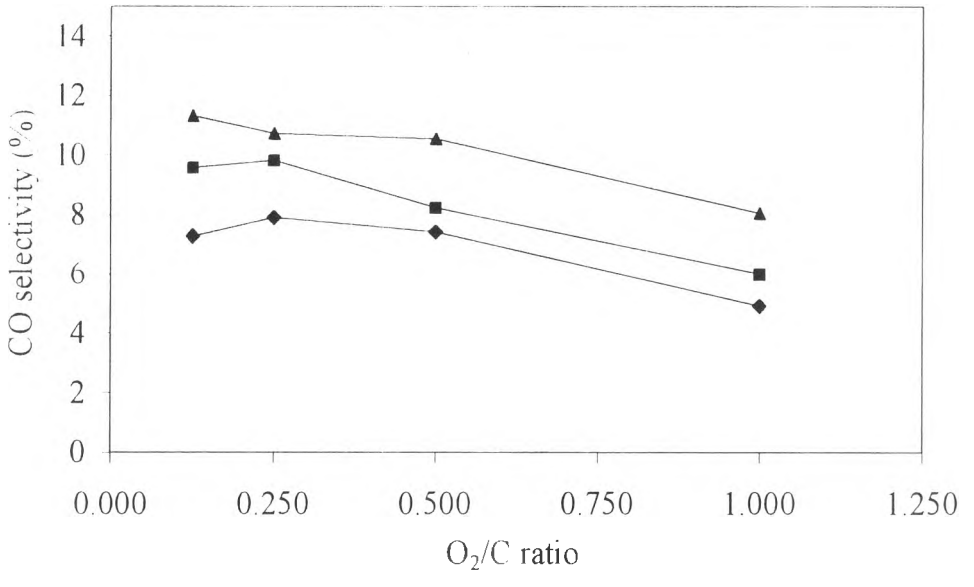

Figure 4.43 The effect of O_2/C ratios on CO selectivity at (◆) 550°C, (■) 600°C and (▲) 650°C over 5%Ni/$Ce_{0.75}Zr_{0.25}O_2$ at H_2O/C = 2/1.

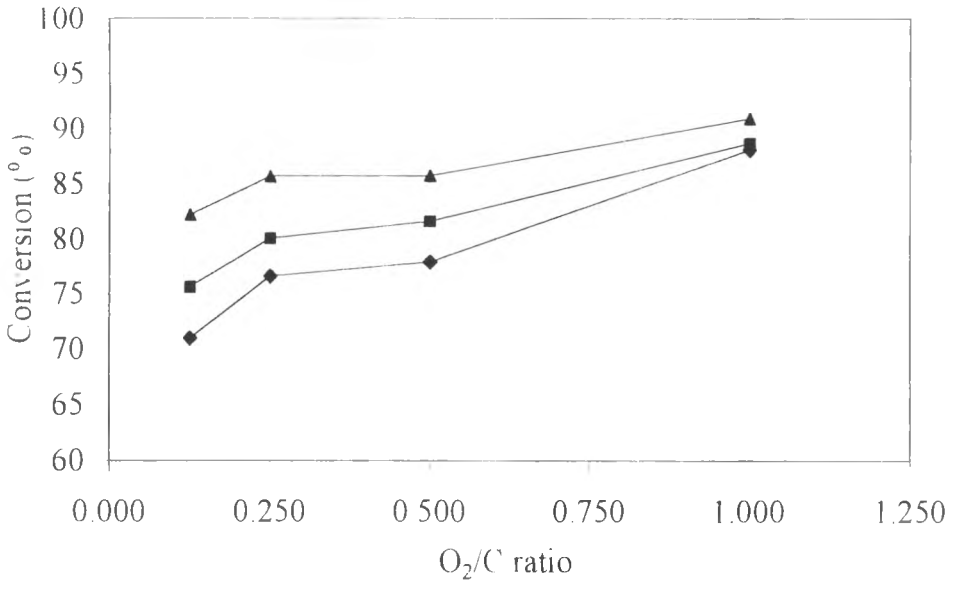

Figure 4.44 The effect of O_2/C ratios on iso-octane conversion at (◆) 550°C, (■) 600°C and (▲) 650°C over 5%Ni/$Ce_{0.75}Zr_{0.25}O_2$ at H_2O/C = 2/1.

4.8 Coke Formation Study

Coke formation study on 5%Ni/$Ce_{0.75}Zr_{0.25}O_2$ with calcined temperature at 500°C was study by using STA and SEM analysis. The reaction was carried at 650°C, H_2O/C ratio = 2/1 and O_2/C ratio = 1/1 for 100 hours. Figure 4.45 shows the activity of 5%Ni/$Ce_{0.75}Zr_{0.25}O_2$ during 100 hours operation. The activity of 5%Ni/$Ce_{0.75}Zr_{0.25}O_2$ gradually changed dropped and reached the final value of the activity of ca. 0.90 after during 100 hours operation. For the product selectivity of H_2 shown in Figure 4.46, the main product is hydrogen. However, the selectivity of H_2 slowly dropped, while the selectivity of CO_2 increased slightly during 100 hours operation.

The spent catalyst was invested coke formation by using Thermogravimetric Analyzer and Scanning Electron Micrograph (SEM). TGA result showed that there was no coke formation since the peak indicated the loss of carbon can not be detected. The SEM can confirm this result. Figure 4.47 shows the SEM pictures of fresh and spent 5%Ni/$Ce_{0.75}Zr_{0.25}O_2$. It is found that no coke formation on spent 5%Ni/$Ce_{0.75}Zr_{0.25}O_2$ when compare to the fresh sample. It is suggesting that 5%Ni/$Ce_{0.75}Zr_{0.25}O_2$ is suitable catalyst for autothermal system since it gives high activity and reduce coke formation.

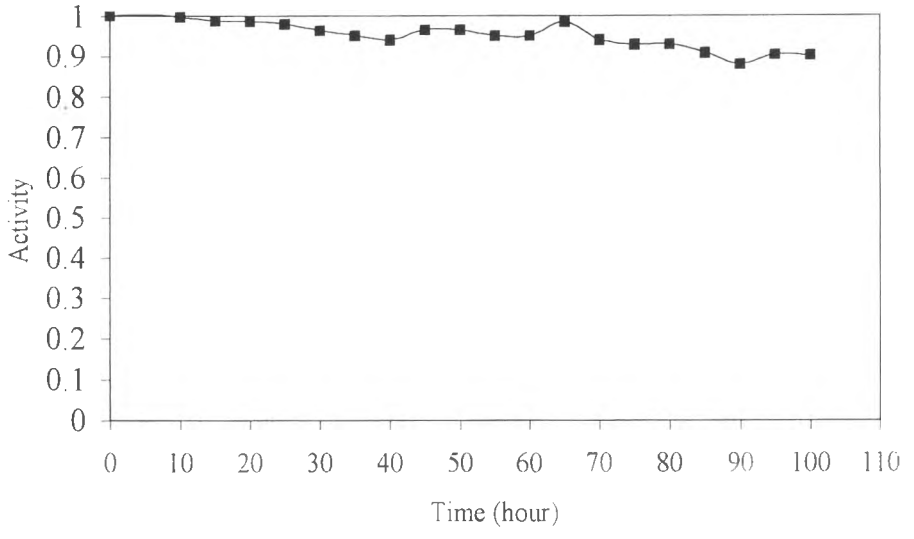

Figure 4.45 The activity of 5%Ni/$Ce_{0.75}Zr_{0.25}O_2$ versus time for coke formation study carried under autothermal system at H_2O/C = 2/1, O_2/C = 1/1 and 650°C.

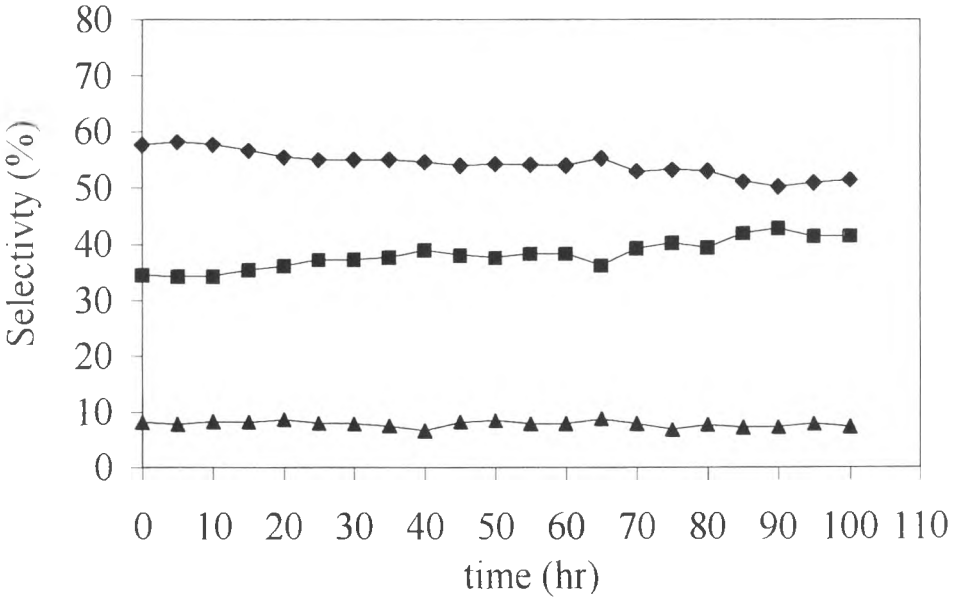

Figure 4.46 H_2, CO and CO_2 selectivity versus time from coke formation study carried under autothermal system at H_2O/C = 2/1, O_2/C = 1/1 and 650°C; (◆) H_2, (■) CO2 and (▲) CO.

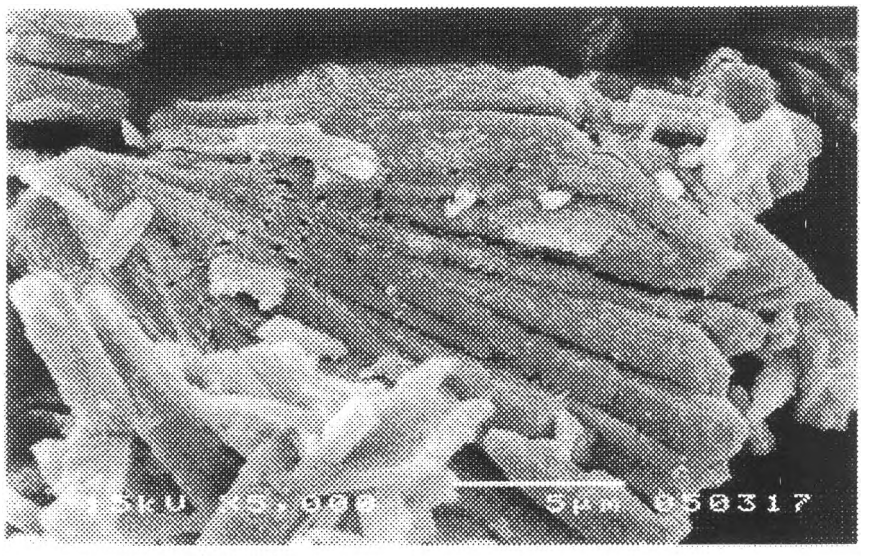

(a)

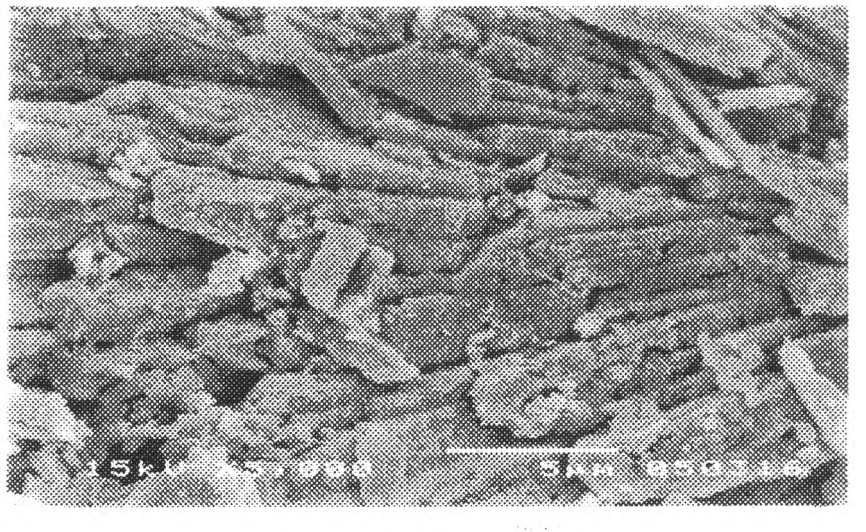

(b)

Figure 4.47 SEM pictures of (a) 5%Ni/$Ce_{0.75}Zr_{0.25}O_2$ calcined at 500°C and (b) spent 5%Ni/$Ce_{0.75}Zr_{0.25}O_2$.